STRAIN ESTIMATION OF FIBRONECTIN FIBRILS USING TWO DIMENSIONAL

DIGITAL IMAGE CORRELATION.

A THESIS IN

Electrical Engineering

Presented to the Faculty of the University
of Missouri-Kansas City in partial fulfillment of
the requirements for the degree

MASTER OF SCIENCE

by

BHARGAV JAVVAJI

B. TECH., Jawaharlal Nehru Technological University, 2011

Kansas City, Missouri

2014

STRAIN ESTIMATION OF FIBRONECTIN FIBRILS USING TWO DIMENSIONAL

DIGITAL IMAGE CORRELATION.

Bhargav Javvaji, Candidate for the Master of Science Degree

University of Missouri-Kansas City, 2014

ABSTRACT

Bone consists of a highly specialized mineralized extracellular matrix (ECM) which supports cells and tissues. Fibronectin is a non-collagenous protein produced by bone cells and is one of the earliest ECM proteins to be assembled. Fibronectin supports the assembly of several other bone matrix proteins, therefore understanding the dynamic process by which the fibronectin is assembled provides insight into how the bone matrix is formed. Live cell imaging of fibronectin assembly in living osteoblasts helps in understanding the kinematics of its assembly, which is a highly dynamic process.

Fibronectin assembly was imaged in 2T3 osteoblasts using time lapse imaging over a 48 hour period. This was divided into four equal 12 hour stages, in which we could observe the assembly process from no fibrils to formation of a mature fibril network. Two Dimensional Digital Image Correlation (2D-DIC), a powerful optical computational tool, was used to quantify the tensile and compressive strains experienced by the assembling fibronectin fibrils due to the extensive cell motion. The 2D-DIC technique was used to quantify the total lengths, large strains and displacements of the assembling fibronectin fibrils. All the code has been developed using Matlab version 12. Seven

different movie stacks from two experiments were analyzed. The results quantify the strains experienced by the fibrils at different time stages, due to the underlying cell motion. The average tensile and compression strains were reduced by 6,000με in the12-24hr movie segment compared to 24-36hr. The average tensile strain was decreased by 6,000 με and the average compression strain was decreased by 3,000με in the 24-36hr movie segment compared to 36-48hr. This suggests that fibril strains are reduced as a consequence of matrix maturation. Individual fibrils also showed unique strain profiles, illustrating both the dynamic nature and heterogeneity of fibril motions. This thesis signifies the importance of fibronectin protein in the ECM assembly process by providing strong mathematical and statistical details obtained using the Digital Image Correlation.

APPROVAL PAGE

The faculty listed below, appointed by the Dean of the School of Computing and Engineering have examined a thesis titled 'Strain Estimation of Fibronectin Fibrils Using Two Dimensional Digital Image Correlation' presented by Bhargav Javvaji , candidate for the Master of Science degree, and certify that in their opinion it is worthy of acceptance.

Supervisory Committee

Ganesh Thiagarajan, Ph. D., P.E., Committee Chair
Department of Civil and Mechanical Engineering

Sarah L. Dallas, Ph. D.,
Department of Oral Biology

Mark L. Johnson, Ph.D.,
Department of Oral Biology

Cory Beard Ph.D.,
School of Computing and Engineering

CONTENTS

LIST OF TABLES

LIST OF ILLUSTRATIONS

ACKNOWLEDGEMENTS

I would like to express my utmost gratitude to my thesis committee chair and main advisor for this research, Dr. Ganesh Thiagarajan for his support and encouragement throughout the length of my research here at University of Missouri – Kansas City. I will never forget his kind concern, sincere and valuable insights as I hurdle all the obstacles in the completion of this work.

I would like to thank my committee member and the main source of funding for this research, Dr. Sarah Dallas and committee member Dr. Mark Johnson and Dr. Cory Beard for their constant support, guidance and encouragement that gave me the motivation to bring this work to its conclusion.

I would wish to express my gratitude towards Aditya Roshan who first worked on this project and introduced me to this research.

I also owe my deepest gratitude to my grandfather Mr. Krishnaprasad Yedla and my parents Mr. Venkateswara Rao and Mrs. Malathi and my brother Arun for their unending love and constant encouragement. It gives me great pleasure in acknowledging the support of my family, friends and the professors throughout the years for their encouragement and support in one way or the other.

CHAPTER1.

INTRODUCTION

The extracellular matrix (ECM) is a three dimensional (3D) structure whose function is to support cells and tissues. The skeleton consists of a specialized mineralized ECM that supports the whole organism and enables locomotion. In order to understand more about the function of ECM, we need to understand the mechanisms by which the ECM is assembled and reorganized. Bone ECM contains fibrillar proteins, such as collagen, fibronectin and fibrillin, which interact with each other and maintain tissue strength **(Sivakumar, et al., 2006)**. Not only does the ECM provide structural support to tissues, but it also controls cell function by regulating cell-matrix interactions and by acting as a repository for storage of growth factors such as transforming growth factor beta (TGF-β), and insulin like growth factor. Thus the ECM can control the availability of growth factors and can modulate growth factor signaling events.

Fibronectin is one of the earliest ECM proteins to be assembled and studies indicate that it acts as an initiator for assembly of other ECM components and is required to maintain ECM stability (for review see **(Dallas, Chen, & Sivakumar, 2006)**. Cellular interactions with the ECM are the basis for fundamental biological processes such as cell adhesion, migration, growth and differentiation (Friedl, 2004). Fibronectin plays an important role in biological processes since it facilitates a variety of cellular interactions with the ECM **(Pankov & Yamada, 2002)**. A number of research studies performed using embryonic fibroblasts derived from the fibronectin-null mice, have confirmed the importance of fibronectin as a key regulator of ECM assembly. For example Velling et al

1

(Velling, Risteli, Wennerberg, Mosher, & Johansson, 2002) showed that the assembly of type 1 and type 3 collagen is impaired in fibronectin null cells and can be rescued by addition of purified fibronectin to the cell cultures. Similarly Sottile and Hocking **(Sottile & Hocking, 2002)** have shown impaired assembly of type 1 collagen and thrombospondin-1. Studies by Dallas et al **(Dallas, et al., 2009)** have suggested a role for fibronectin in regulating matrix deposition of TGF-β by regulating matrix incorporation of latent transforming growth factor beta binding proteins (LTBP-1) into the matrix. They have further shown that the continual presence of fibronectin is required for the continued assembly of bone ECM**.** These studies emphasize the importance of fibronectin as a regulator of assembly of other ECM proteins and have motivated studies of fibronectin fibril assembly dynamics using live cell imaging under the fluorescence microscope.

Live cell imaging is used to understand the nature and properties of living cells by observing the dynamics of the cells **(Live Cell Imaging, 2014).** Previously most studies were performed using static images like light or electron microscopy, which can be combined with bio-chemical analysis, but this provides only a "snapshot" of events at one particular time point. Advances in imaging technologies have led to the use of dynamic imaging which gives deeper insight into the kinetics of the biological specimen under study **(Friedl, 2004)** . Dynamic Imaging has enabled the visualization of both temporal and spatial changes and also collection of biochemical and biophysical information in living specimens like cells. It also allows quantitation of the cellular behavior over time**.**

Research studies have developed pH-sensitive dyes, recombinant fluorescent proteins and other fluorescent probes that can be used to label various structures inside or outside the cell (including the ECM) in live specimens. Dynamic live cell imaging has

been successfully used to image these fluorescently tagged molecules. This thesis uses live cell imaging to investigate the dynamics of fibronectin assembly with a focus on analyzing quantitatively the kinematics of the fibronectin assembly process.

Time lapse imaging of living osteoblasts has shown that fibronectin fibril assembly occurs through the pooling together of fibril units assembled on the cell surface to form larger fibrils **(Sivakumar, et al., 2006)**. Using dynamic imaging of fluorescently tagged ECM molecules, these authors have also shown the highly dynamic nature of ECM fibrillar networks and shown that matrix fibers are constantly stretched/contracted due to the tensile and compression forces of the cell and tissue motion **(Dallas, Chen, & Sivakumar, 2006).** To further understand the kinematics of fibronectin assembly, this thesis focuses on measuring the deformation characteristics of the fibronectin fibrils from time lapse movies during their assembly and the subsequent maturation of the matrix.

There are many methods developed for analyzing images captured using dynamic imaging techniques. Different techniques are used to observe the dynamics of the cell and fibril motion of which Two Dimensional Digital Image Correlation (2D-DIC) is a reliable and effective method. We have used this method for quantifying the strains on the fibronectin fibrils. Other methods that could be used include the Particle Image Velocimetry (PIV) technique, which is a correlation process used by Zamir et al **(Zamir, Czirok, Rongish, & Little, 2005)** to map the deformation fields in tissue material points in various layers of the avian embryo. PIV based algorithms were also developed by **(Kim, Yoon, Kim, & H. H. Chun, 2006)** to study the three dimensional topology of the turbulence velocity field. Lu and Cary **(Lu & Cary, 2000)** have developed a DIC method

to calculate larger deformations in the specimen under study by using the second order approximations of the deformation gradients.

We have opted to use the 2D DIC method for the computational analysis of time lapse movies of fibronectin fibril assembly. DIC is a cheap non-contact and yet accurate solution for measuring strains and displacements and is simple to use compared to other techniques, such as the speckle interferometery technique **(McCormick & Lord, 2010).** Interferometric techniques use coherent light source and the deformation is measured by recording the phase difference of the scattered light wave from the test object surface before and after deformation **(Pan, Qian, Xie, & Asundi, 2009).** In contrast non-interferometric techniques such as DIC determine the surface deformation by comparing the gray intensity changes of the object surface before and after deformation **(Pan, Qian, Xie, & Asundi, 2009)**. DIC technique uses the natural surface of the specimen to calculate the deformation and requires conventional digital photography **(McCormick & Lord, 2010)**.

The second chapter of this thesis deals with the methods and the materials used to image the fluorescently tagged ECM molecules and also provides an overview of the 2D DIC method. It discusses the modifications that have been made to the existing DIC code to improve the analysis and also the organization of the results.

The third chapter discusses the development of the protocol for the analysis of fibronectin fibril kinematics. It outlines the step by step procedure that has been used in performing the final digital image correlation analysis. It discusses the advantage of each step of the protocol. This protocol can be followed for any movie stack of fibronectin

assembly thus providing a standard method that can be used to quantify the tensile and compression strains acting on the fibrils due to the cell motion.

The fourth chapter discusses the application of the modified 2D DIC and use of the protocols developed in chapters 2 and 3 to perform analysis and quantify the strains, lengths and displacements of the fibrils on two different movie experiments termed FN_24 and FN_12.

The last chapter discusses the conclusions based on the results obtained in chapter 4 and provides comments based on the quantifications of the tensile/compression strains of fibronectin fibrils during their assembly, the individual strain profiles of fibrils and changes in fibril dynamics over time. The significance of these strain values from a biological perspective is also discussed, as well as future work that can be implemented in this research.

CHAPTER2.

DEVELOPMENT OF THE DIC ALGORITHM FOR MEASURING FIBRONECTIN

FIBRIL STRAINS DURING ASSEMBLY

2.1   Overview of Live Cell Imaging:

The time lapse imaging, which demonstrates the formation of fibronectin fibrils in osteoblasts, was performed in the Dallas lab prior to the work performed in this thesis. The current study used image stacks generated from these previous experiments as the data source for the DIC analysis. The experiments were performed using the 2T3 osteoblast cell line. This is an immortalized cell line obtained from transgenic mice expressing the SV40 T-antigen under control of the bone morphogenic protein-2 (BMP2) promoter **(Dallas, et al., 2009)**. Because of its similarity to primary osteoblasts (i.e. osteoblasts freshly isolated from bone tissue) and its capacity to produce a similar extracellular matrix, - the 2T3 cell line is a good model for primary osteoblasts.

Fibronectin assembly was imaged using a probe consisting of purified human fibronectin tagged with alexafluor555 (a red fluorescent dye). The reagents and protein labeling kits were purchased from Invitrogen Corporation, Carlsbad, CA. For live imaging of fibronectin, 2T3 cells were plated into glass coverslip bottomed chamber slides (Nalge Nunc, Rochester NY) at a density of $2x10^4$ cells/cm^2 in culture media consisting of α-Minimal Essential Medium (α-MEM) supplemented with 10% Fetal Bovine Serum, 2mM L-glutamine and 100U/ml penicillin/streptomycin. After the cells were allowed to adhere overnight, Alexa 555-labeled fibronectin (5ug/ml) and unlabeled fibronectin (5ug/ml) were added in 2ml fresh α-MEM.

6

Time lapse imaging was performed using a Nikon TE 2000E microscope under widefield epifluorescence and differential interference contrast illumination. This automated imaging system is maintained at a constant temperature of 37ºC and 5% CO_2 using a temperature control system and automated gas mixer system from Life Imaging Services, (Reinach, Switzerland), in conjuction with a custom plexiglass incubation chamber that encloses the microscope. The microscope hardware and image acquisition were controlled by the "Metamorph" software (Universal Imaging Corporation, PA).

Z-stack images were acquired for each time point under 20X magnification in fluorescence mode and also under differential interference contrast illumination using a Roper Scientific Coolsnap HQ cooled CCd camera with 12-bit grey scale resolution. Fields of 448 x 335μm were imaged at spatial resolution of 696 x 520 pixels (2x2 binned mode) every 20 minutes for 48 hours from 5 optical planes with 1.5 μm separation between planes. Image stacks were exported as 8 bit image stack (.stk) files.

When acquiring images from multiple imaging fields, the motorized microscope stage moves to bring the appropriate imaging field into the camera field of view. While this has the advantage that more data can be generated per experiment from multiple imaging fields, it also introduces rigid body motion (analogous to "camera shake") into the image stacks, due to small variations in the stage position return between time points. The rigid body motion was corrected using an open-source software called image J **(Biomedical Imaging Group, 2011)** using the "stackreg" plugin, which uses an algorithm to register/align the stack of image slices **(Thévenaz, 2011)**. After completing the stack registration the images were cropped to 296x396 pixels only for certain movies if there was rotation at the edges. To better understand and analyze the fibronectin fibril

7

movies, the brightness and contrast were also adjusted. These corrected image stacks provided the input data for the DIC analysis described in this thesis.

Two different experiments were performed on the 2T3 osteoblasts on which the 2D DIC analysis was performed. The names of the experiment are FN_24 and FN_12. The FN_24 movie was acquired over a time period of 48 hours in which images were captured for every 15 minutes thus making a total of 192 frames. The FN_12 movie was also acquired over a time period of 48 hours but the images were captured every 20 minutes, making a total of 144 frames.

2.2 Overview of 2-D Digital Image Correlation:

2D DIC is the most widely used and accepted computational technique to calculate full in plane displacements experienced by a specimen under mechanical loading **(Pan, Qian, Xie, & Asundi, 2009)**. The automated DIC code used in this research was originally developed by Eberl and Thompson **(Eberl, Thompson, & Gianola, 2006)** to calculate the displacements and later modified by Aditya Roshan to calculate the strains experienced on fibronectin fibrils (Roshan, 2011). Additional features have been added to enhance the capabilities of the source code. This chapter provides a detailed description of the additional features added to the code.

Since fibronectin fibrils experience strains at the micro and nano level scale one can use a high magnification microscope in combination with 2D DIC to compute the strains and displacements experienced by the fibrils. 2D DIC is one of the techniques that calculates in plane displacements by correlating the pixels in a search window (square window) before and after a deformation-that occurs due to the external tensile and compression forces acting on the specimen under study **(Pan, Qian, Xie, & Asundi,**

2009). The 2D DIC technique uses the white light speckling pattern to determine the deformation and is more effective than the laser light speckle pattern due to the fact that the laser light has a decorrelation effect **(Brillaud & Lagattu, 2002).** Another important advantage of 2D DIC is the ease of the camera setup i.e. the specimen surface under test must be normal to the optical axis and that is the only condition that needs to be satisfied while capturing the images. This is the reason that 2D DIC is best suited for the current application.

The time lapse imaging of fibronectin assembly in 2T3 cells consists of a stack of images which are captured using the high magnification microscope. These images show the fibronectin fibril maturation from 0 hours to 48 hours. Figure 2.1 shows 5 images at 0, 12, 24, 36 and 48 hours from which we can observe the rapid growth of fibrils from no fibrils at zero hour to a well formed fibronectin fibril network by 48 hours. The fibrils appear to be rapidly breaking and joining in the first 12 hour segment of the movie and as time gradually passes the fibrils become more stable with less breaking and joining but they experience tensile and compression forces due to the cell motions. Depending on the experiment (either FN_24 or FN_12) the images were captured for every 15 minutes or 20 minutes. These images were then computationally analyzed using the developed 2D DIC program which is explained in detail in the following section.

We can clearly observe from Figure 2.1 that the time lapse imaging using fluorescently tagged fibronectin shows no fibril formation at the start of experiment, progressing to a fairly well formed network by as early as 12 hours. The fibril network appears relatively stable from 12 hours onwards.

0h

12h

10

24h

36h
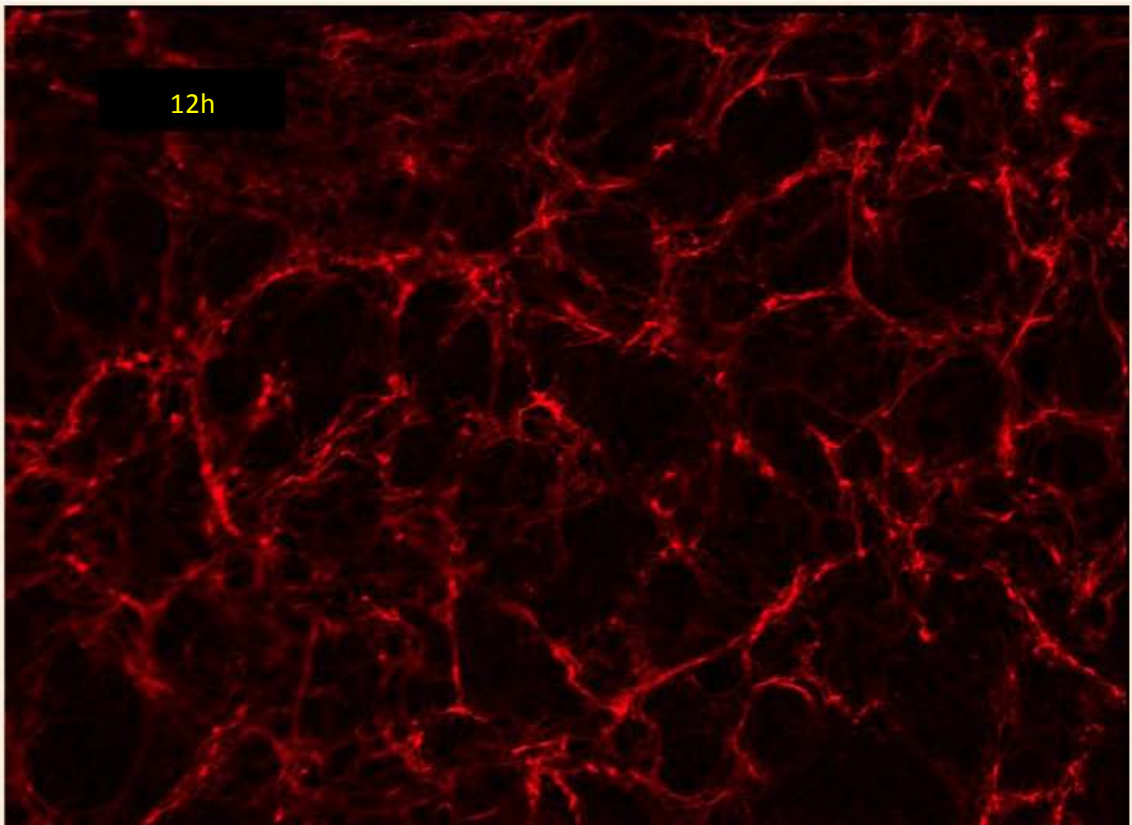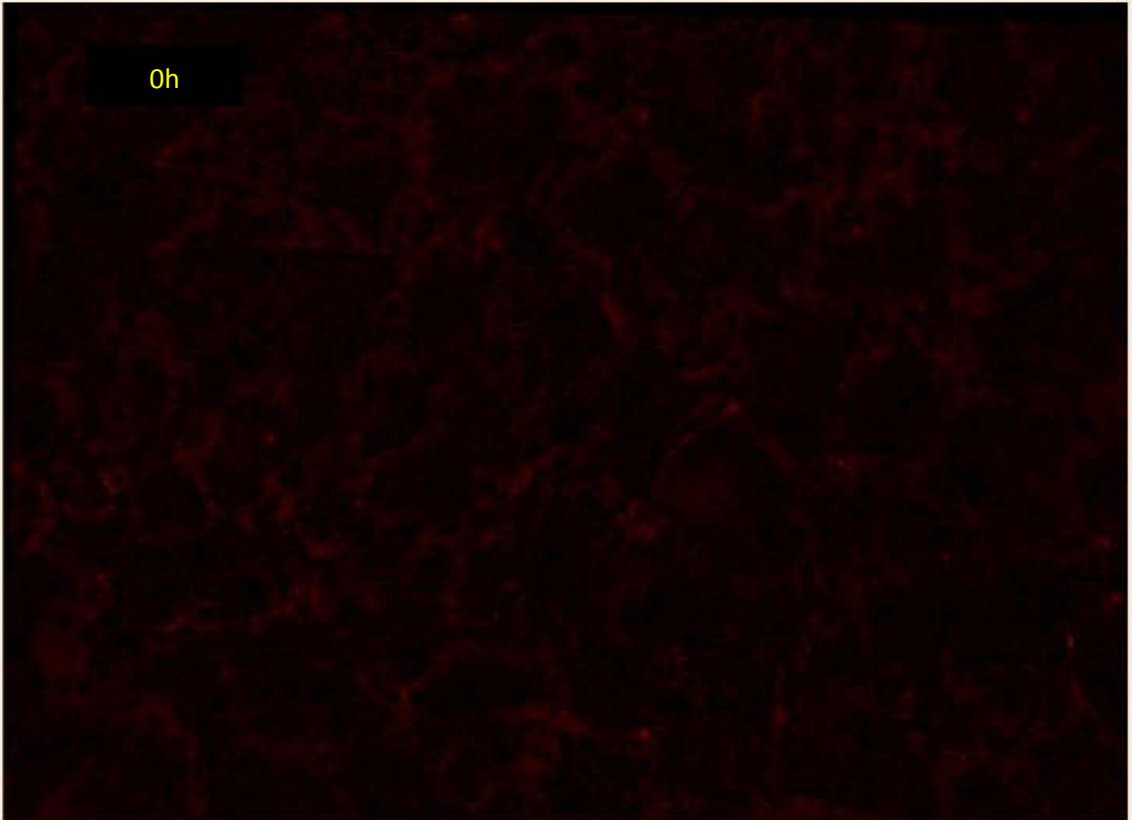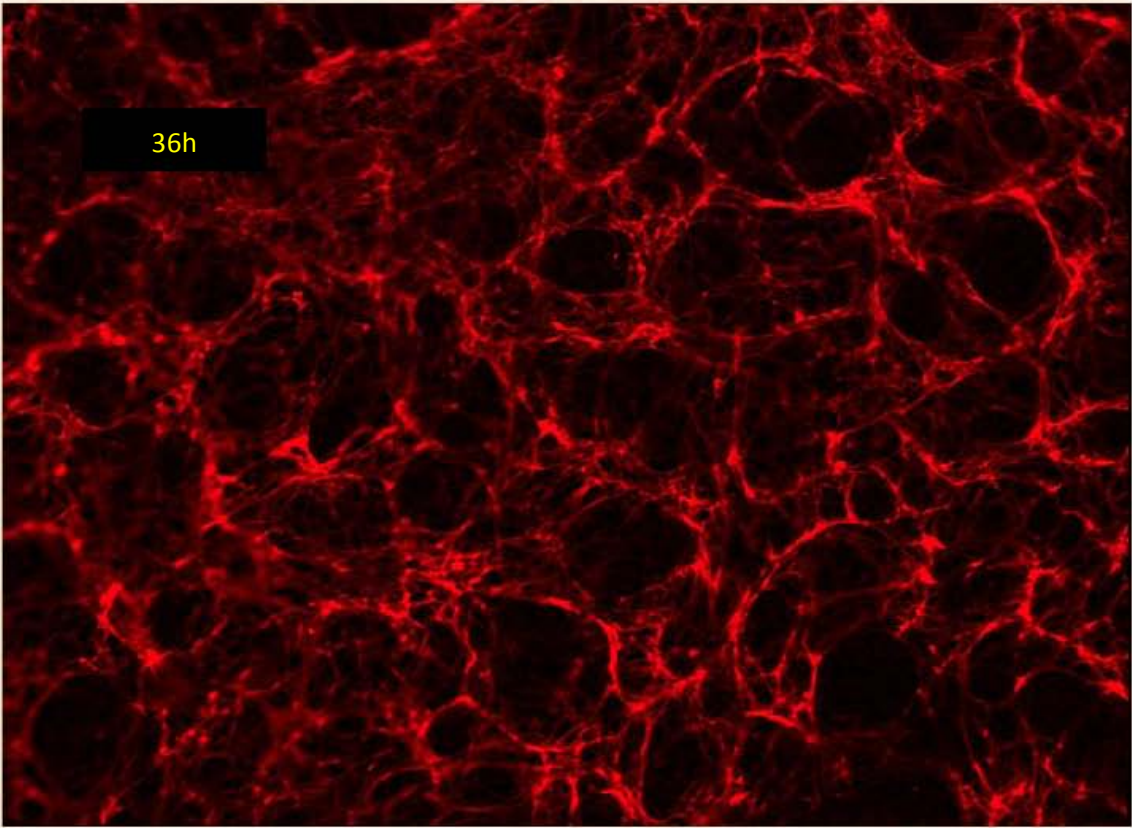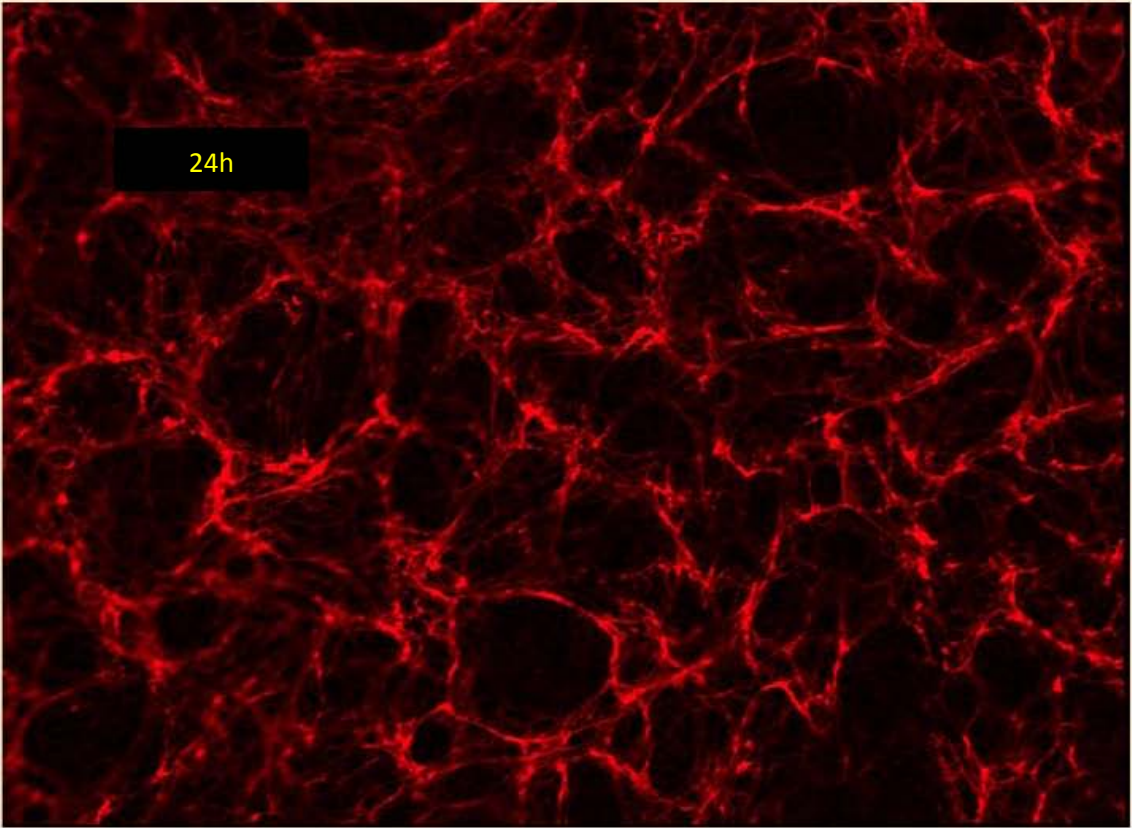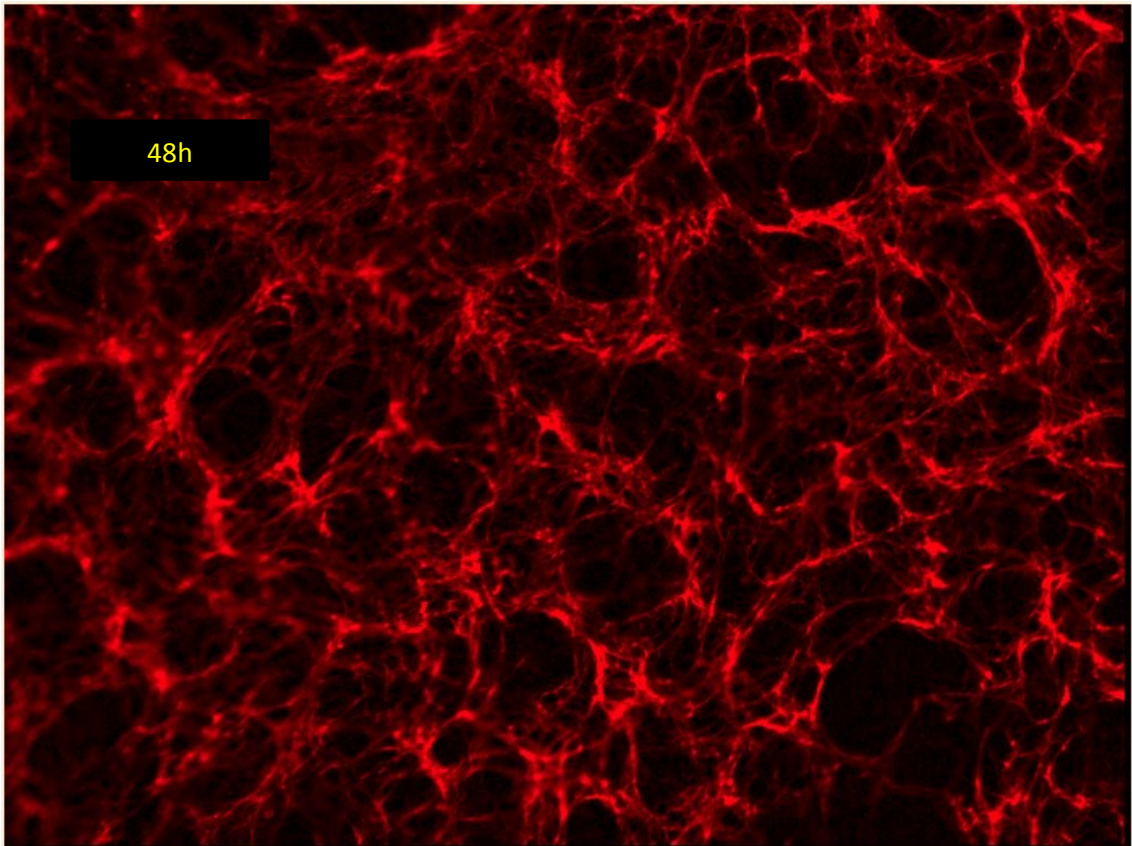
Figure 2- 1: Images captured at 0th, 12th, 24th, 36th and 48th hour of the Time lapse experiment

Once we obtain the registered image stacks, the contrast and brightness are adjusted for all the experiments so that there is no loss of information regarding the deformation of the specimen. The final step is calculating the in plane displacements from the deformation information from the sequence of images using 2D DIC.

The basic principle of the 2D DIC is that it tracks a group of pixels with similar intensity values before and after the deformation by comparing pairs of "before and after" digital images. The correlation is achieved by creating a subset around the pixel of interest in the undeformed image and then trying to find the same subset in the deformed image by predefining a cross correlation criterion and then finding the peak in the distribution of the correlation coefficient which gives the measure of the correlation

12

between the two subsets before and after deformation and thus finding the position of original pixel in the deformed image.

For this application we used the Normalized Cross Correlation (Lewis, 1995) which is defined in the equation 2.1.

$$\gamma(u, v) = \frac{\sum_{x,y}[f(x,y) - \bar{f}_{u,v}][t(x - u, y - v) - \bar{t}]}{\{\sum_{x,y}[f(x,y) - \bar{f}_{u,v}]^2 * \sum_{x,y}[t(x - u, y - v) - \bar{t}]^2\}^{0.5}} \qquad (2.1)$$

Where,

$\gamma(u, v)$ is cross correlation coefficient;

f is the image;

$\bar{t}$ is the mean of the template;

$\bar{f}_{u,v}$ is the mean of $f(x, y)$ in the region under the template;

t is the image feature under correlation.

2.3   Description of the Program:

The 2D DIC code developed by Eberl and Thompson **(Eberl, Thompson, & Gianola, 2006)** is a powerful computational procedure for quantifying the dynamic properties experienced by biological molecules that are captured using dynamic imaging. This technique was modified by Aditya Roshan **(Roshan, 2011)** to suit the application of finding the deformations experienced in fibronectin fibrils due to cell motions. This section gives a thorough description of the code which was further modified in the current study to add improved features to the code developed.

The Matlab program has four Matlab scripts which have to be executed in the following order.

13

2.3.1 File List Generator:

This script helps the user to select the stack of digital images on which the normalized cross correlation is performed. When this script is executed it generates a .mat file which has the labels of all the images that are to be correlated and the output .mat file and can be accessed by any other script. The first condition for the input to this script (i.e. the filename of images) is that they follow a specific pattern which is of the form 'Xx.extension', where X denotes a string that can be any combination of ASCII characters which should be constant for all the images, and x denotes a number that is unique to each image. The second condition is that the set of images being processed are in an ascending sequence i.e. x (current image) – x (previous image) =1 for all concurrent images. The '.extension' could consist of a variety of file types like tiff, jpeg, png, gif and all other file formats accepted by Matlab®.

The function has two options of selecting images either Automatic or Manual as shown in figure 2.2.

14
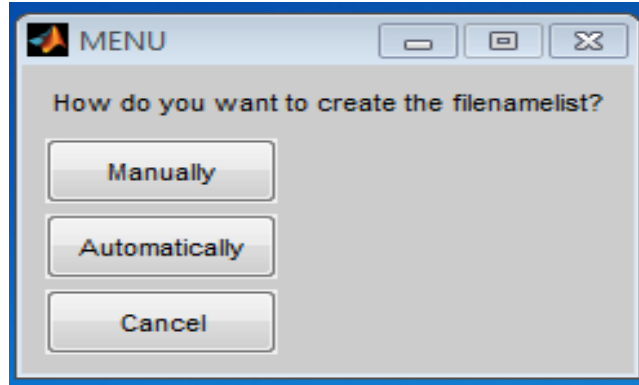
Figure 2- 2: Option for selecting the list of file names

If the 'Automatic' function is chosen then the user selects the first image and the function automatically gives the names to the subsequent images by incrementing the number.

If the 'Manual" option is selected the function accepts all filenames without any constraints on the number of characters or digits in it. The user selects the first image and the last image from a selection window. The names of these strings are stored in separate variables and are tested where all the characters are denoted by a 1 if it is an alphabet and a 0 if the character is a non-alphabet. The function then searches for the '.' character in the entire string. Since the value of the image number is located just before '.', a counter is used to count the value of each character backwards until an alphabet (i.e. a value of 1) is reached. This counter value gives the image number values of the first and the last image and these values are used to generate all the image names that are located in between these two values. The image names are then stored, in a single column, in a matrix file called 'filenamelist.mat'. The other functions that need to access to the image list can load this .mat file into their workspace and work on these images.

15

2.3.2 Grid Generator:

The main function of this script is to select the fibrils and specify the number of raster points required by each fibril. Whenever the user runs the grid generation program it generates a menu option as shown in figure 2.3 where the user can select fibrils with different shapes but since the fibrils do not have a specific geometrical shape we normally choose the 'Manually select markers' option. After the manual option is selected the user has to specify the number of fibrils that need to be correlated as shown in figure 2.3 and the number of raster points required by each fibril and all this data gets saved in number_s.dat which is a row matrix where the first column indicates the total number of fibrils selected which is say N, the second column indicates the number of raster points for fibril 1, the third column indicates the number of raster points for fibril 2 and the $(N+1)^{th}$ column specifies the number of raster points of Nth fibril. Once the numbers are specified the user then places the yellow '+' shaped markers on the fibrils for the base image which is designed to be always the first image of the filenamelist.mat. To keep track of the number of raster points that have been placed the title of the base image changes dynamically thus showing the user the number of points required for the fibril. The user also has the flexibility to replace the selected markers if he/ she wishes to place them more precisely.
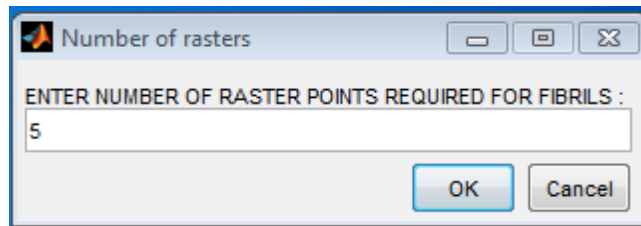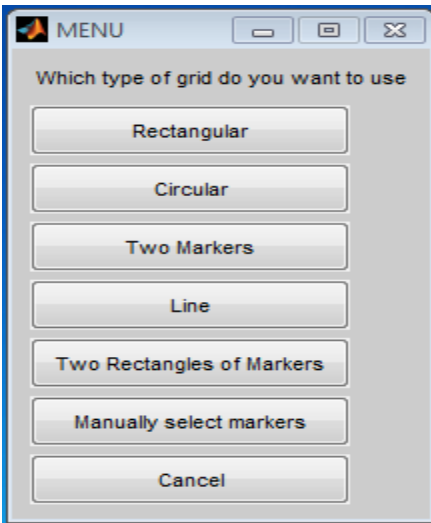
Figure 2- 3: The different shapes of fibrils that the user can
choose and number of RP required by each fibril

All the points that have been selected on the base image are stored to files called 'grid_x.dat' and 'grid_y.dat', where grid_x.dat contains the x-coordinates of the base points selected and grid_y.dat has the y-coordinates of the base points selected. Figure 2.4 shows a zoomed in version of a fibril that has been selected for correlation. This image is also saved in the displacement_tracking folder that was created when the grid was selected.

The main advantage of this code is that it allows the user to position different numbers of raster points on different fibrils rather than having a set number of raster points per fibril that does not take into account the variations in fibril length. This is an improvement on the code developed by Aditya Roshan. In this way the user can

17

position a larger number of raster points on longer fibrils and a smaller number of raster points on the shorter fibrils, which saves computational time to calculate the strains. In the current study, we determined that there was an optimum density of raster points per unit length of the fibrils (please see chapter 3) to provide the best accuracy.

2.3.3   Correlation:

This function is used to track the motion of the fibrils due to the cell motion.
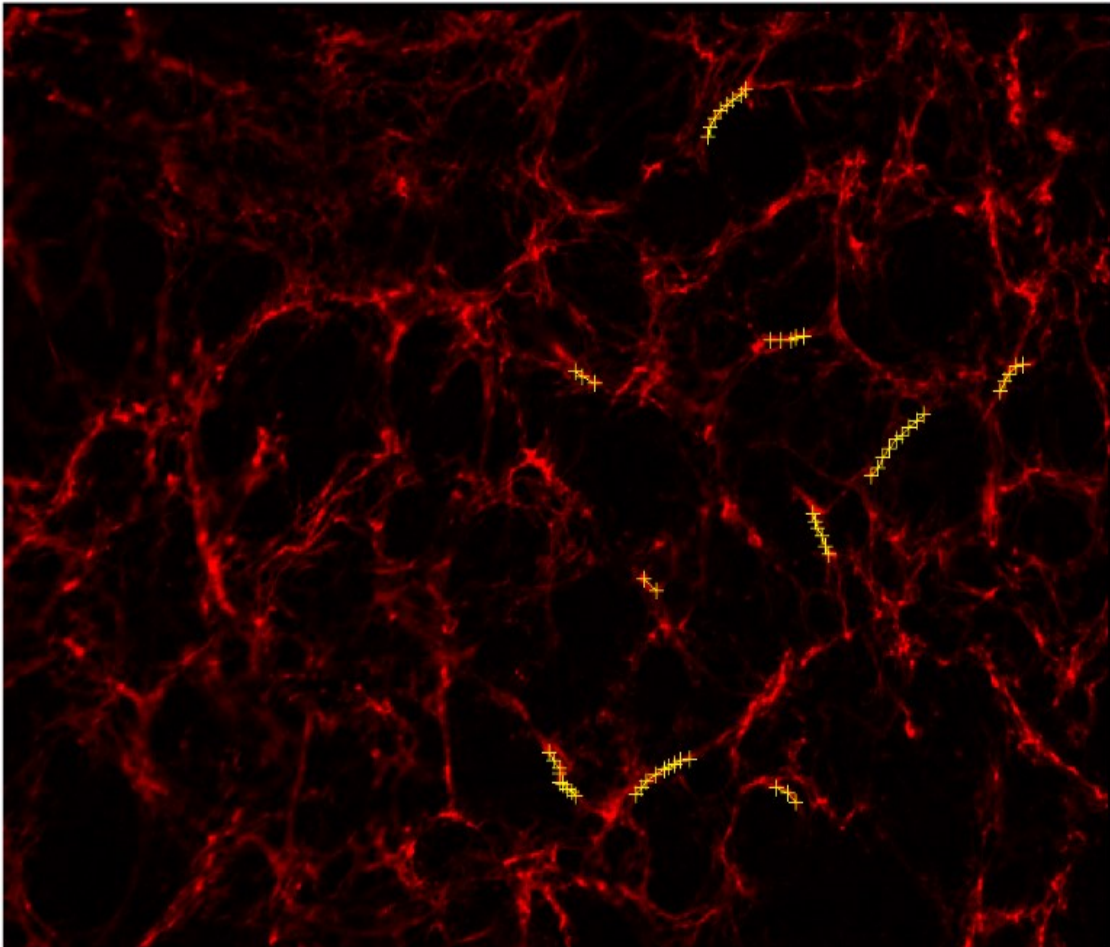
Figure 2- 4: Position of raster points on base image

It takes in the filenamelist.mat and grid_x.dat, grid_y.dat as the input files, because this function needs the details of the base image which is always the first filename in filenamelist and the coordinates that were selected in the base image for correlation which is stored in *gridx* and *gridy*. Correlation function also needs the number_s.dat file which has information regarding the number of raster points selected for each individual fibril.

Once these files are loaded the function enters a loop where it selects two images, one being the base image (the first image of filenamelist) and the other being the current image (second image of filenamelist). It then creates a square window around the points that were selected on the base image using variable_grid_generator and then compares the pixel intensity values to the intensities in the current image using normalized cross correlation, thus finding the position of the new points in the current image after the deformation. The reason for selecting a square subset instead of just picking the original pixel is based on the assumption of deformation continuity –i.e. that the grayscale values of the neighbors of a pixel remain the same in both the deformed and undeformed image and it also gives more constraints that will differentiate from other subsets. These new positions of the raster points in the current image are saved in the files called valid_x.dat and valid_y.dat which are the x and y coordinates respectively. After each iteration the base image is updated to the current image and the current image is updated to the next image in the filenamelist which had started from second image.

The *cpcorr1* function also allows the user to update the window size by just changing the number of the *corrsize* variable in the function depending on the magnitude of the movement of the fibrils. If we change the window size to say 10 then it creates a

19

22x22 matrix of pixels around each raster point on the base image and a 44x44 matrix of pixels in the current image and then performs a normalized cross correlation which helps to locate the position of the new raster points in the current image.

2.3.4 Strain Calculation:

This function is used to calculate the strain values between the individual raster points and also the large strains and total lengths of the fibrils. This function calculates the deformation gradient between two points as explained.

In Figure 2-5 the two end points of a line segment whose initial positions are 'a' and 'b' and assume that some kind of compression or tensile force which acted on the line segment has caused it to change its shape, thus forming a new line segment with new end points denoted by 'A' and 'B' respectively.
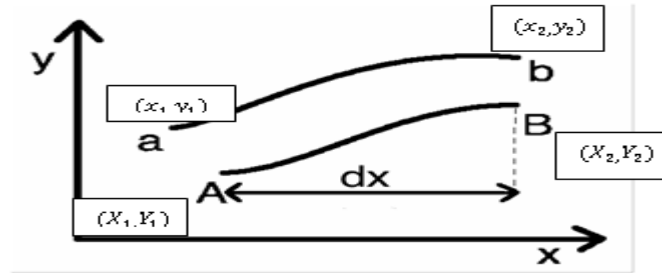
Figure 2- 5: The coordinates of the end points of fibrils before and after deformation

We define 1D vector of coordinates as

$$[dA] = \begin{bmatrix} X_1 \\ Y_1 \end{bmatrix} \quad ; \qquad [dB] = \begin{bmatrix} X_2 \\ Y_2 \end{bmatrix}$$

$$\text{(2.2)}$$

$$[da] = \begin{bmatrix} x_1 \\ y_1 \end{bmatrix} \quad ; \qquad [db] = \begin{bmatrix} x_2 \\ y_2 \end{bmatrix}$$

The initial points 'a' and 'b' are transformed into 'A' and 'B' due to

deformation. Therefore we can write the deformed and undeformed positions using the

linear coordinate transformation equation as shown in the equation 2.3.

$$[dA] = [F][da] \qquad \text{and} \qquad [dB] = [F][db]$$

$$\text{i.e.} \begin{bmatrix} X_1 \\ Y_1 \end{bmatrix} = \begin{bmatrix} F_{11} & F_{12} \\ F_{21} & F_{22} \end{bmatrix} \begin{bmatrix} x_1 \\ y_1 \end{bmatrix} \qquad \begin{bmatrix} X_2 \\ Y_2 \end{bmatrix} = \begin{bmatrix} F_{11} & F_{12} \\ F_{21} & F_{22} \end{bmatrix} \begin{bmatrix} x_2 \\ y_2 \end{bmatrix} \qquad (2.3)$$

Where [F] denotes the deformation gradient matrix.

Now we can solve equation 2.3 using the 'linsolve' function available in Matlab

which takes two sets of coordinates which are the initial and final positions of the points

and the transformation matrix is calculated which is known as the deformation gradient

matrix. Once this matrix is calculated we can calculate the engineering strains on the

line segment in two directions i.e. horizontal and vertical using the equation 2.4.

$$E_{11} = \frac{1}{2}(F_{11}F_{11} + F_{21}F_{21} - 1)$$

$$E_{12} = \frac{1}{2}(F_{11}F_{12} + F_{21}F_{22})$$

$$E_{21} = \frac{1}{2}(F_{12}F_{11} + F_{22}F_{21})$$

$$E_{22} = \frac{1}{2}(F_{12}F_{12} + F_{22}F_{22} - 1)$$

where,

E_{11} represents the axial elongation,

E_{22} represents the transverse strain and

E_{12} and E_{21} represents the shear strain.

These engineering strains are calculated between each set of two raster points on

the fibril. The function goes into a loop for each fibril starting from the first frame where

it takes the position of the deformed and undeformed points and calculates the

21

individual strain. The loop is completed once it calculates all the strains between each individual set of raster points for all the fibrils for all the frames. These values are stored in the def_grad folder where it contains folders named as fibril numbers each containing the deformation gradient and engineering strains starting from first frame for each individual set of raster points.

This function also calculates the large strain on the fibrils and the total length of the fibrils. The total length of the fibril is calculated using the location of new raster points which are stored in *validx* and *validy*. We load this data into two variables and access them in such a way that we calculate the distance between two consecutive raster points in a fibril in the current image using equation 2.5.

$$len = \sqrt{((v_{x(i+1)} - v_{x(i)})^2 + (v_{y(i+1)} - v_{y(i)})^2)} \qquad (2.5)$$

Where, $v_{x(i+1)}$ is the X-coordinate of the second point

$v_{x(i)}$ is the X-coordinate of the first point

$v_{y(i+1)}$ is the Y-coordinate of the second point

$v_{y(i)}$ is the Y-coordinate of the first point

Once we find the length between two consecutive raster points in a fibril we accumulate this length with the lengths between all the consecutive points in a fibril in the current image thus giving us the total length of the fibril in the current image. This process is repeated until we find the total lengths of all the fibrils in all the frames where we performed the DIC.

The large strain is calculated using equation 2.6.

$$Large\ strain = \frac{(l_1^2 - l_0^2)}{(2 * l_0^2)} \qquad (2.6)$$

Where, l_1 is the total fibril length in the current image.

l_0 is the total fibril length in the base image.

This formula is used to calculate the large strain of a fibril in the current image using the total lengths of the fibril in the current image and the total length of the fibril in the base image, it was concluded from Aditya's thesis **(Roshan, 2011)** that optimum accuracy in results are achieved for calculating the large strains if we use the previous image as the base image. This process is repeated until we find the large strains of all the fibrils in all the frames used in the 2D DIC analysis.

CHAPTER3.

PARAMETRIC ANALYSIS

3.1   Introduction:

This chapter introduces the parameters that affect the calculations of the total

lengths and large strains of different fibrils which have been simulated using the two

dimensional digital image correlation algorithm developed. The number of raster points

selected for a fibril is an important parameter which is used in quantifying the lengths

and strains in the 2D DIC method.

The chapter is organized into two different sections which describe the additions

made to improve the efficiency of the code. In the first section we introduce the idea of

variable raster point density and explain in detail its advantages over fixed raster point

density and perform a comparison of results from the two approaches. The second

section helps to develop a protocol for selecting the number of raster points required by

the fibrils based on their lengths which should be applicable for any similar image stack.

3.2   Fixed Raster Point Density:

This section introduces the calculation of strains and the total lengths of the fibrils

using the predefined number of raster points which was in the original 2D DIC code. For

this analysis the fibrils were classified into three types depending upon their physical

length as small (10-20 pixels), medium (25-55 pixels) and large (60-90 pixels) fibrils.

Once we divided the fibrils into these three types, then we selected one individual fibril

from each of these categories and applied a fixed raster point density of five points for

any fibril selected from any of the three- categories.

3.3   Variable Raster Point Density:

This section explains the calculation of strains and the total lengths of the fibrils using the variable raster point density, which is the modification that enhances the capabilities of the original code. For this analysis the fibrils were classified into three types depending upon their physical length as small, medium and large as described in the above section. We then selected the same three fibrils that were selected for the fixed raster point density analysis but varied the number of raster points positioned on the fibril, depending on its length.

3.4   Comparison Steps:

The comparison step is used in understanding the differences between the fixed and variable raster point densities. The scripts that have been used to make the comparison of fixed and variable raster point density are described below.

3.4.1. File List Generator:

This script is used to select the image range from a stack of images that will be used to select the fibrils. We used the image range 108 to 144 for comparison purposes since it was observed that the fibrils are more mature and stabilized at this later stage of the movie when compared to other stages where the fibrils are still being formed and/or there is breaking or joining of fibrils. Once we selected this image range for our analysis we stored the names of all the image names in the filenamelist.mat file and saved it in the same folder where it can be accessed by other scripts.

3.4.2. Grid Generator:

We use this script for selecting the number of fibrils to be analyzed and number of raster points to be positioned on each fibril. All the fibrils were selected from the first image of filenamelist.mat file which is the base image for this particular simulation. We selected one fibril from each of the three predefined categories i.e. small, medium and large and performed the analysis of both fixed and variable raster point densities for each of these three individual fibrils.

Figures 3.1 and 3.2 show the fibrils that were selected under the small, medium and large categories respectively and illustrate the positioning of the fixed number of raster points compared to variable number, based on the fibril length. Table 3-1 summarizes the fibrils and the numbers of raster points that were positioned on them using the fixed or variable raster point analysis.

Table 3- 1: Distinguishing fibril into fixed and variable densities

Fibril number(Category)	Fixed density fibrils	Variable density fibrils
Fibril 1(Small)	5	3
Fibril 2(Medium)	5	10
Fibril 3(Large)	5	17
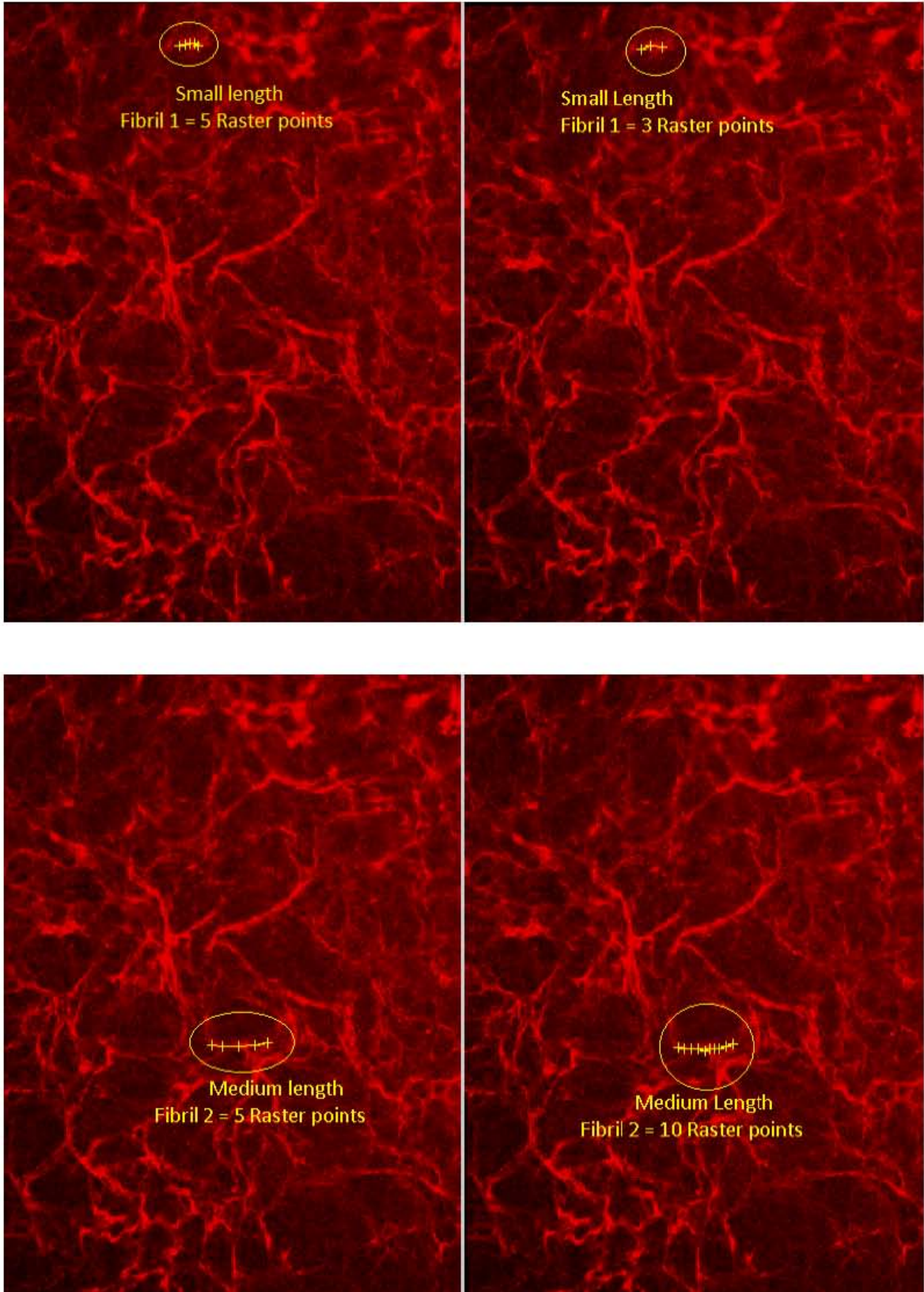
Figure 3- 1: Fibril 1(small) and Fibril2 (medium) with fixed and variable densities
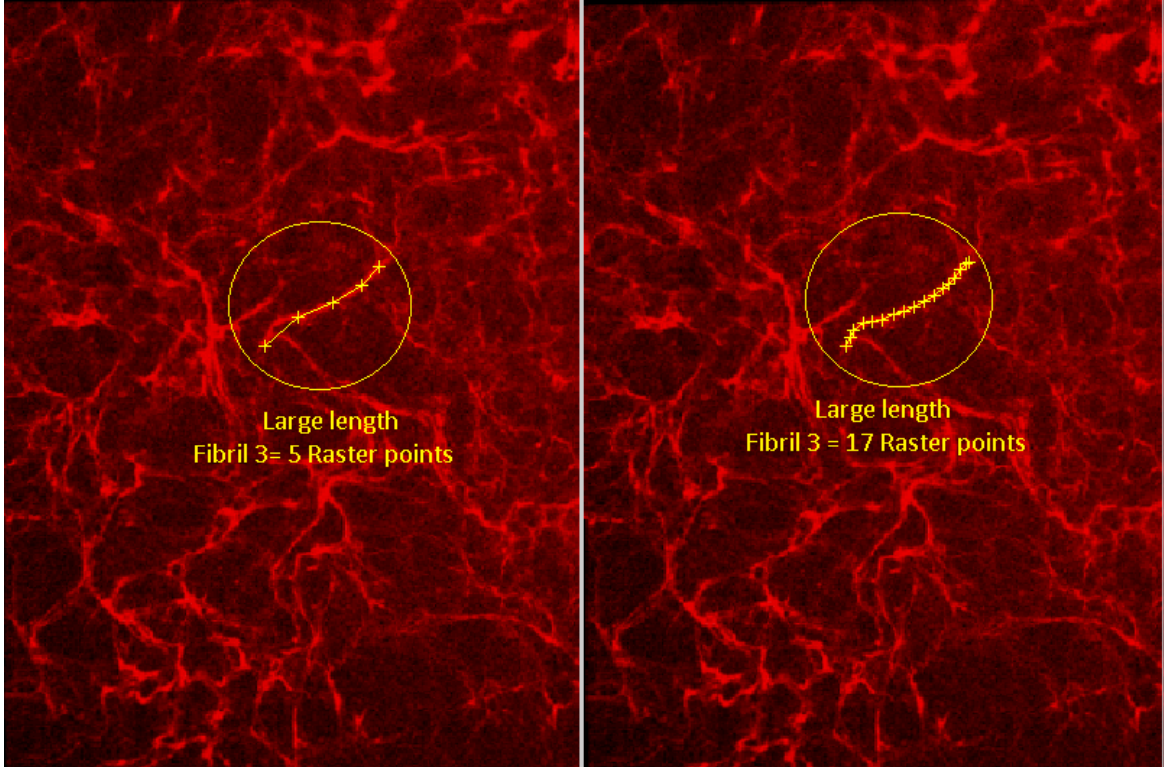
Figure 3- 2: Fibril3 with fixed density of 5 and variable density of 17 raster points

3.4.3. Automate Image:

Once the fibrils are selected using either the fixed or variable raster point densities the coordinates of all the raster points are stored in grid_x and grid_y and information regarding the total fibrils and number of points for each fibril is stored in number_s. These data files are loaded into the automate image function where the correlation takes place with respect to the previous image. The automate image function goes into a loop and in the first iteration it takes the base image which is image 108 in this case and loads the grid_x and grid_y on to the base image which are the yellow markers.

Once this data is loaded it correlates these points on the base image with the current image which is image 109 in the first iteration using the *cpcorr* function where a

window of 5 pixels is selected thus creating a search window of 11x11 pixels in the base image and a search window of 22x22 pixels in the current image. Then we use normalized cross correlation to find the x and y coordinates of new points in the current image which are saved in *validx* and *validy*. This iteration is continued until image number 143 becomes the base image and image number 144 becomes the current image. The tracking of the points is saved in the displacement tracking folder which is a stack of images that represent the tracking magnitude and direction using the *quiver* function. The *quiver* function is applied on the new positions which are indicated as green colored '+'signs whereas the original raster points are yellow colored '+' signs. The yellow arrows illustrate the magnitude and directionality of the displacement.

3.4.4. Workspline:

Once we find the position of the new location of the raster points in the images using normalized cross correlation we run the *workspline* function, which computes the strains and the total lengths which quantifies the 2D DIC. This function takes in the *validx* and *validy* data which are the new positions of the raster points after cross correlation for each image pair and uses this coordinate data to calculate the deformation gradient and also the total length. Once we find the total length we find the large strain using the equation 2.6.

3.4.5. Comparison of Lengths and Large Strains using Fixed and Variable Densities:

The large strain and total length results are acquired after we run the simulation using the fixed and variable raster point densities. The results are organized in an easy way that- the comparison is done for the same fibril which is simulated using fixed and variable densities. Figure: 3.3 shows the total length and large strain of the small length

fibril using the fixed density of five raster points and the variable density of three raster points. The data shows that this particular fibril showed only a small variation in the length. The graphs plotted using the high (five) and low (three) raster point densities appeared very similar, suggesting that there is no appreciable increase in accuracy of the strain estimations by increasing from 3 to 5 raster points on a small fibril (10-20 pixels).
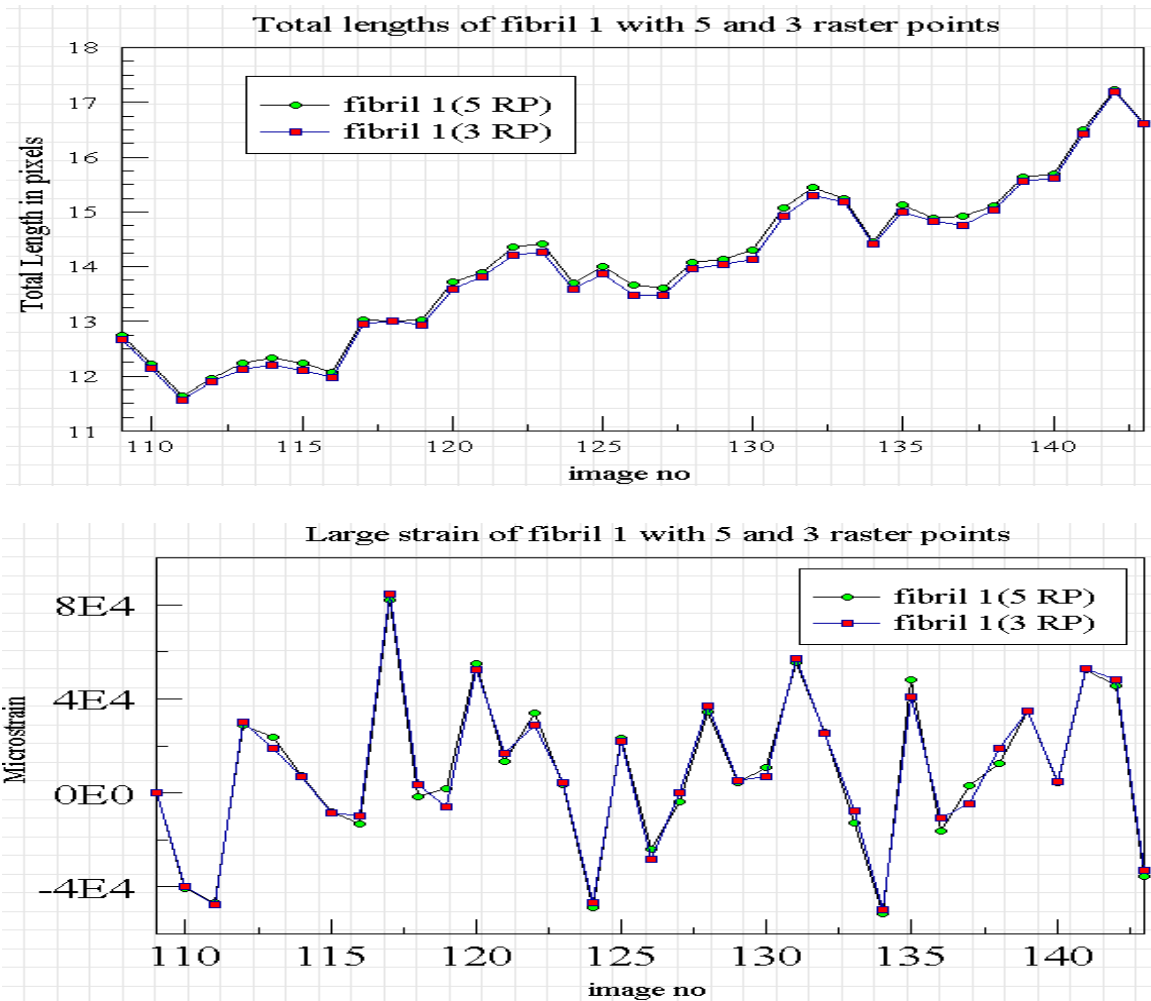
Figure 3- 3: Fibril3 with fixed density of 5 and variable density of 17 raster points

Figure: 3.4 shows the total length and large strain of the medium length fibril using the density of five raster points and the density of ten raster points. In this case, there is a 20% difference in the computations of the fibril lengths and the strains with the lower (five) raster point density compared to the higher (ten) raster point density. By using ten raster points instead of five, the analysis captures small variations in fibril length which were not detected using 5 raster points.
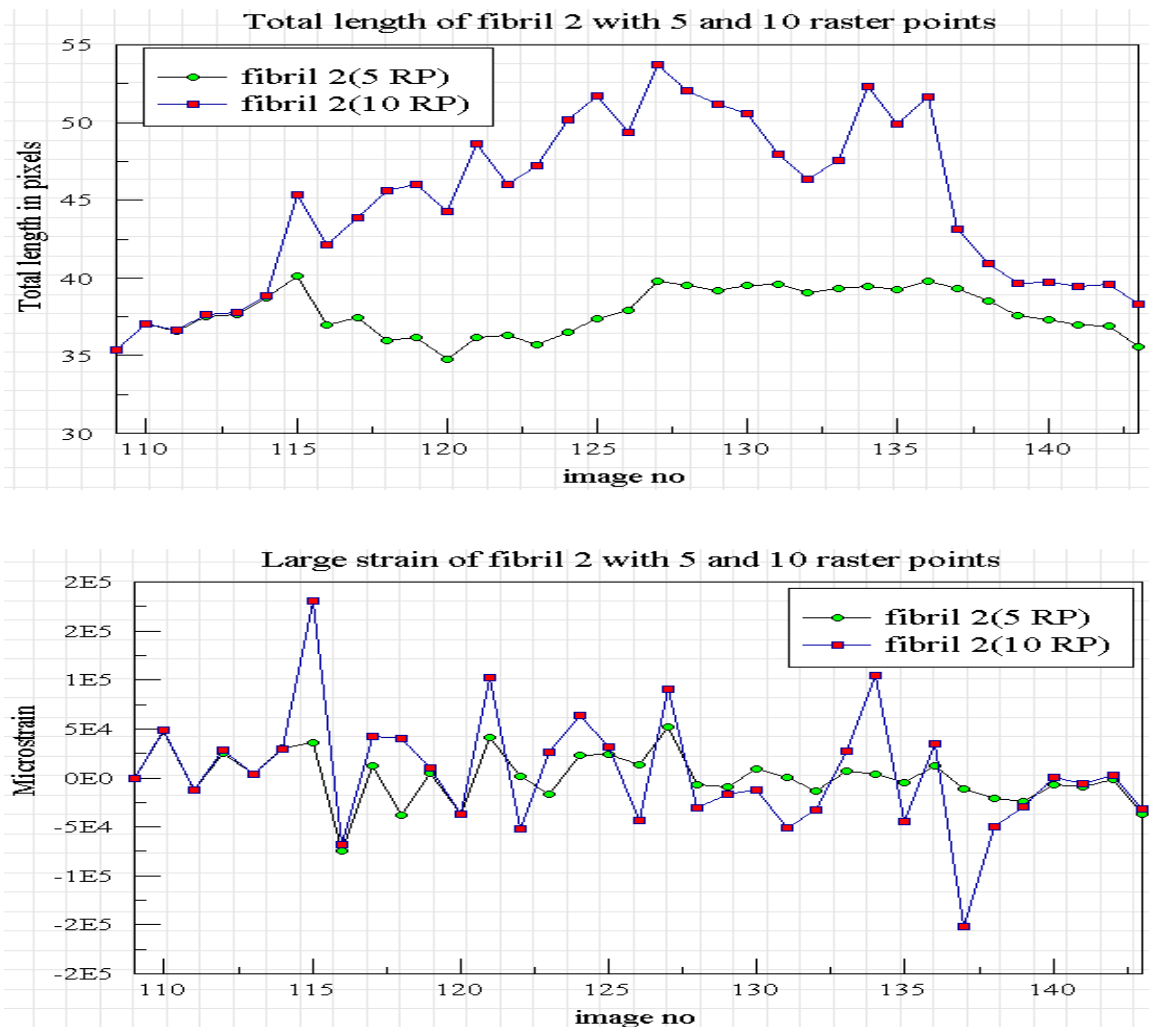
Figure 3- 4: Total length and large strain of fibril 2 with fixed density of 5 and variable density of 10

Figure 3.5 shows the total length and the large strain of the large length fibril using the fixed density of five raster points compared to the variable density of seventeen raster points. The graph shows that using seventeen raster points captures smaller variations in length that are not detected when only 5 raster points are used. This leads to considerable discrepancies in the strain profiles of the fibril calculated using five raster points vs. seventeen raster points. The data suggest that the variable raster point density, in which the raster number can be increased in relation to the fibril length, provides greater sensitivity for measuring fibril deformations.
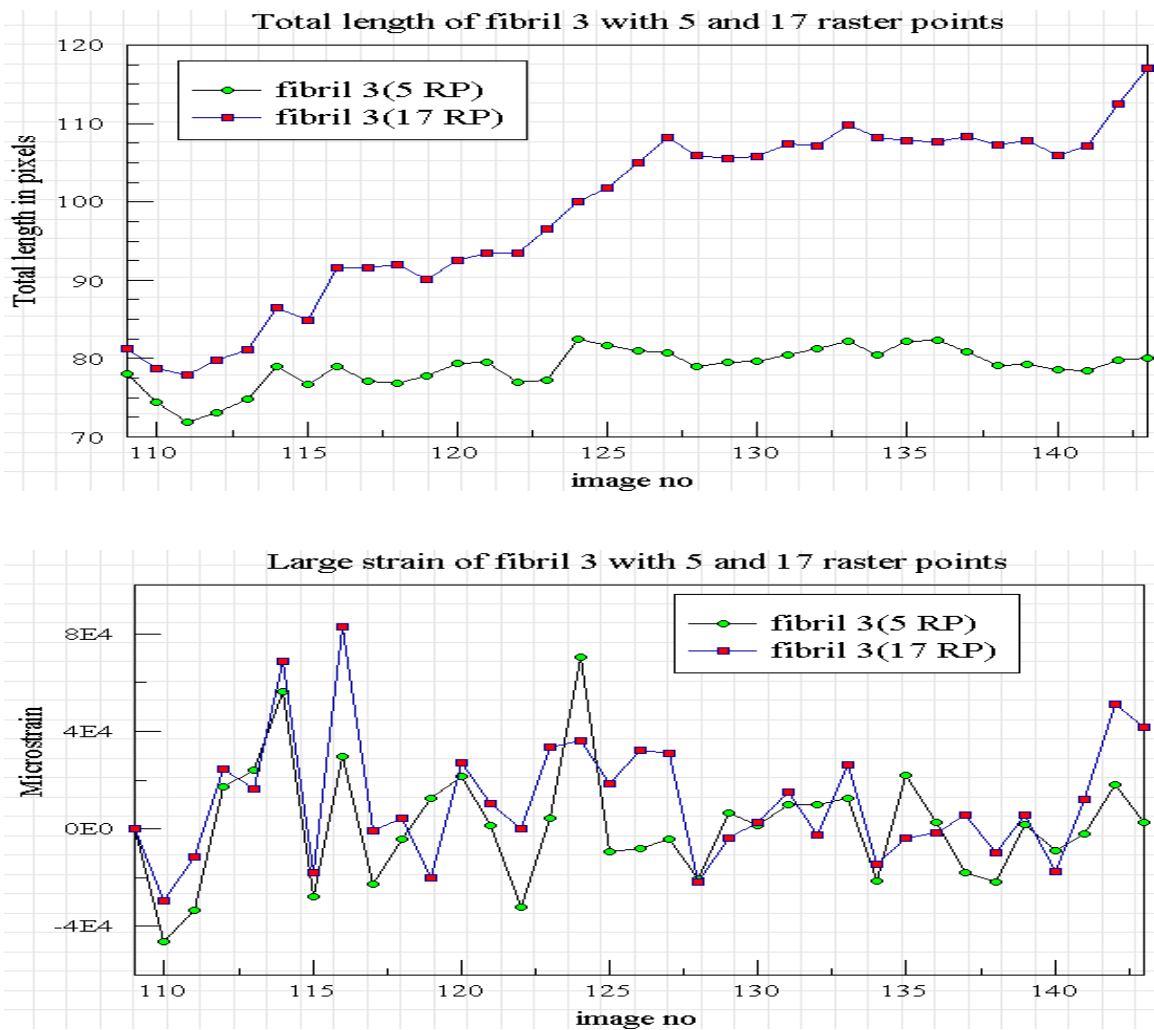
Figure 3- 5: Total length and large strain of fibril 3 with fixed density of 5 and variable density of 17

Together these validation studies show that variable raster point density is a better way of calculating the total lengths and large strains as it gives the user the flexibility to use more raster points for longer fibrils, and that a fixed raster point density might result in underestimation of the fibril deformations, particularly for larger fibrils.

3.5   Raster Point Density Convergence:

After concluding that variable raster point density improves the code, we next wanted to determine if there is an optimum number of raster points that could be used for any given fibril i.e. is there a raster point density per unit length of fibril at which a saturation point is reached. If so, what is the maximum density of raster points per unit length of fibril?

This section discusses the effect of different densities of raster points on strain measurements in fibronectin fibrils. For this purpose we split the fibrils into three different categories of small, medium and large (as defined previously) and selected one fibril from each category. Different raster point densities were then applied for the same fibril to determine if there was a saturation point at which there was no further increase in accuracy with increasing raster density.

The analysis was first performed on a small fibril from a movie stack using the last 12 hour segment of the movie. Different densities of raster points were applied to the same fibril and the total lengths were calculated. Figure: 3.6 shows the small length fibril used for the analysis with different densities.
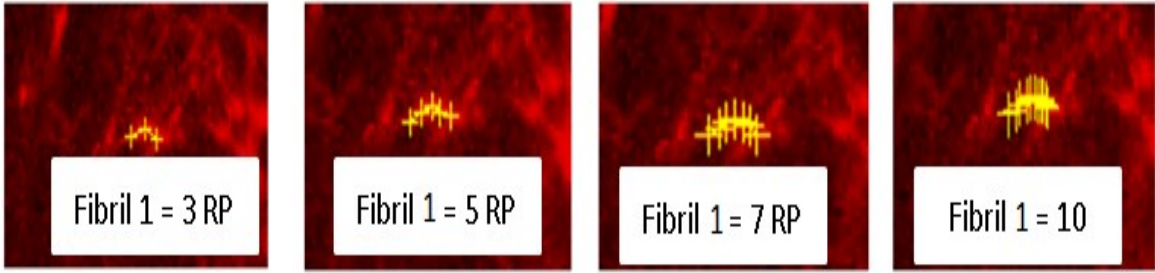
Figure 3- 6: Small length fibril with different densities of 3, 5, 7 and 10 raster points

After selecting the fibril for analysis, the physical length of the fibril was calculated using the coordinate information of the raster points which is stored in *gridx* and *gridy*. The physical length of fibril 1 for the first image frame was calculated to be 14.33 pixels. Now the length of the fibrils is calculated using the computational approach for the same first image frame in Matlab. The results are shown in the table3-2:

Table 3- 2: Physical length and Computational Length for small length (fibril 1) fibrils

	Physical length calculated(Pixels)	Computational length(Pixels)	Length/RP
fibril 1(3 RP)	14.33	14.861	14.861/5=2.97
fibril 1(5 RP)	14.33	15.193	15.193/5=3.03
fibril 1(7 RP)	14.33	15.284	15.284/5=3.05
fibril 1(10 RP)	14.33	15.954	15.954/5=3.19

We can observe from the above table that the range of the lengths calculated computationally is 14.861 to 15.954 pixels and the actual physical length of the fibril is 14.33 pixels. Therefore, the fibril with three raster points resulted in a computed length closest to the physical length. This suggests that there is no need to select additional raster points for the fibril, since increasing the raster density increases the computational time. We initially assumed of using one raster point per five pixels since that gave minimal difference when we calculate computational length/raster point value shown in

fourth column of Table 3-2.

Figure: 3.7 illustrates the total length in pixels and the large strain in micro strain for all the different raster point densities that have been used for the fibril. We can observe that the raster point densities of 3, 5, and 7 calculate similar length and strain values, and the density of 10 raster points shows a positive offset by 2 pixels length when compared to the other three densities. This suggests that the three raster point density is sufficient to provide accuracy for a fibril of 14.33 pixels in length. This led us to the assumption that using a raster point density of 1 raster point for every 5 pixels of fibril length might be optimum for calculating fibronectin fibril lengths and strains.
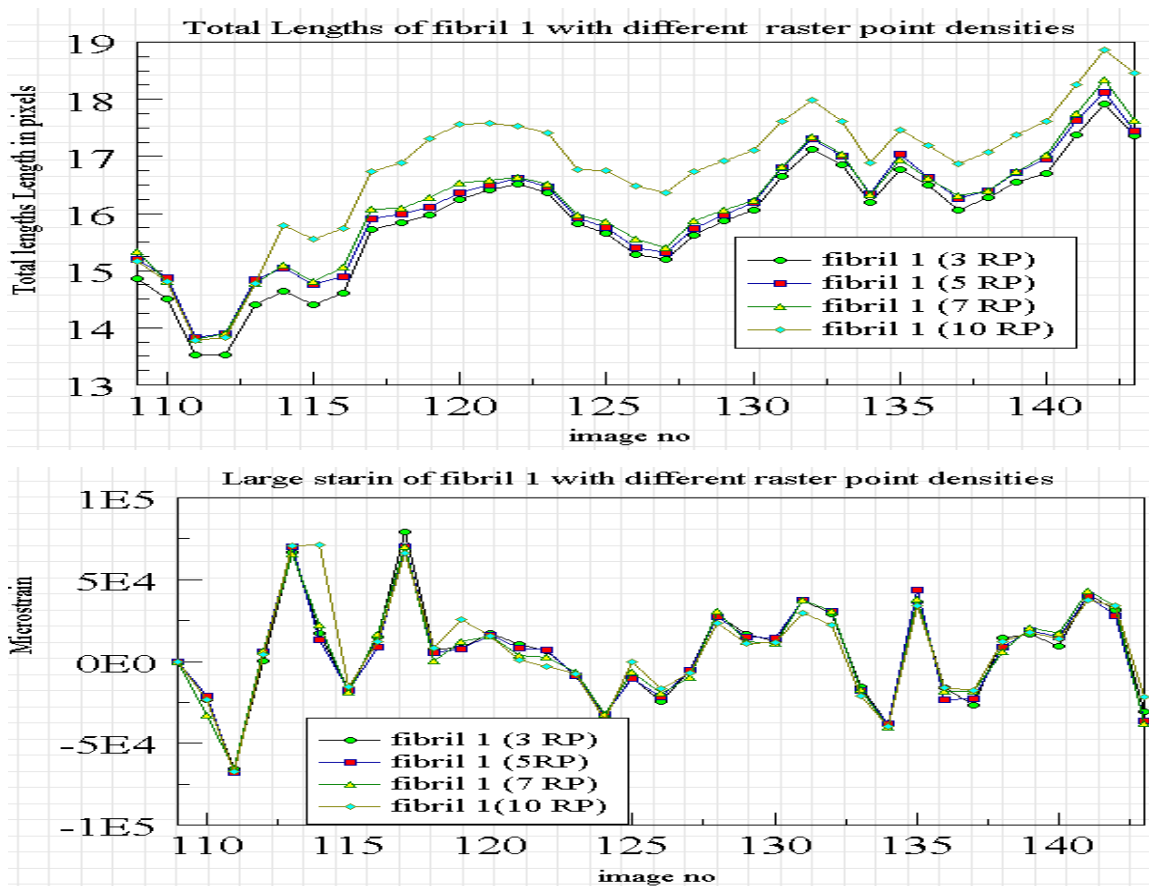
Figure 3- 7: Total Length and large strain for different densities of fibril 1

We tested this five pixel per raster point assumption for two more fibrils, where one of them was selected from the medium length category and one from the large category. The medium length fibril (fibril 2) had a physical length in the first image frame calculated at 26.23 pixels and the large length fibril (fibril 3) had a physical length in the first image frame of 52 pixels. By following the same assumption of 1 raster point per 5 pixels in length, these fibrils should give optimal results using 5 and 10 raster points respectively. Table 3-3 shows the computational lengths for fibril 2 using raster point densities ranging from 5-11 and the computational lengths for fibril 3 using raster point densities ranging from 10-18. Note that the computational length of fibril 2 (5 RP) and fibril 3 (10 RP) calculated for the same first image frame was close to the physical length.

The table below shows the physical and computational lengths of fibril2 and fibril 3 respectively:

Table 3-3: Physical length and Computational Length for medium (fibril 2) and large length (fibril 3) fibril

	Physical length calculated (Pixels)	Computational length (Pixels)	Length/RP
fibril 2(5 RP)	26.53	26.245	26.245/5=5.24
fibril 2 (7 RP)	26.53	26.332	26.332/5=5.26
fibril 2 (9 RP)	26.53	26.878	26.878/5=5.37
fibril 2 (11 RP)	26.53	27.124	27.124/5=5.42
fibril 3 (10 RP)	52.4	50.140	50.14/5=10.028
fibril 3 (12 RP)	52.4	50.349	50.349/5=10.06
fibril 3 (15 RP)	52.4	50.974	50.974/5=10.19
fibril 3 (18 RP)	52.4	51.443	51.443/5=10.28

For fibril 2 the density of 5 points resulted in a calculated length that was 98% of the physical length and for fibril 3 the density of 10 points resulted in a calculated which was 95% of the physical length. Based on these observations we can suggest that a raster

point density of 1 for every 5 pixels of fibril length provides sufficient accuracy for measurements in fibrils of different lengths without unnecessarily increasing the computational time. This new protocol was therefore followed for all the simulations performed on the two different experiments presented in chapter 4 of this thesis.

3.6   Stack Registration:

Stack registration is one of the tools that are applied to the time-lapse image stacks before we perform the normalized cross correlation. This operation is performed because for the time lapse imaging experiments the images are captured from multiple imaging fields using a motorized microscope stage. This leads to some degree of rigid body motion in the image stack due to small variations in the return position of the stage for each time point (which appears similar to "camera shake"). To correct for this rigid body motion a stack registration operation was performed which aligns the boundary of all the images. This was performed using Image J **(Thévenaz, 2011)**, which is an open source software, using the plugin called stackreg.

To illustrate the importance of correcting for rigid body motion, the 2D DIC analysis was performed on a fibril using images which were not stack registered and the total lengths and strains were calculated. The stack registration was then performed on the same image stack and the 2D DIC analysis was performed to calculate the length and strain. The results of this comparison are shown in the figure3-8.
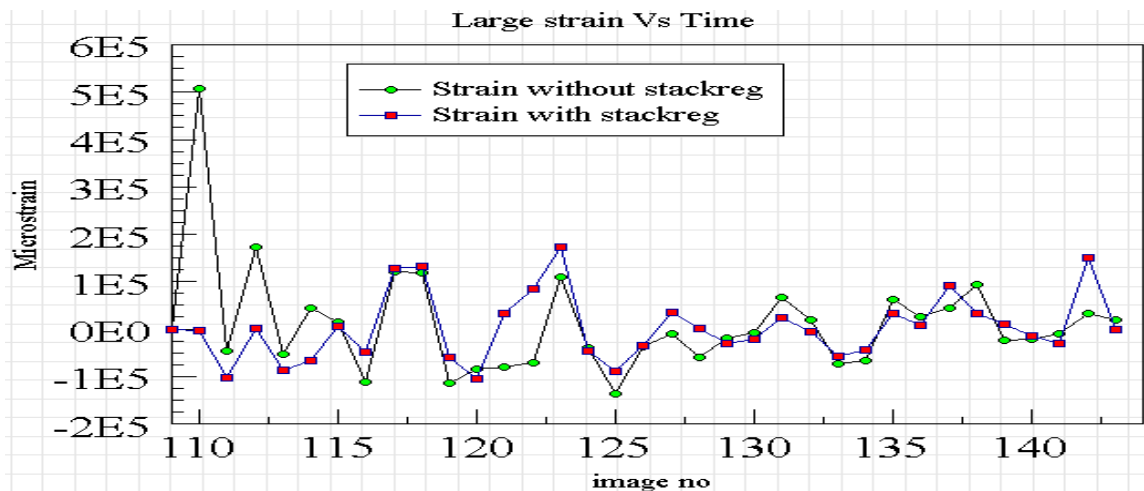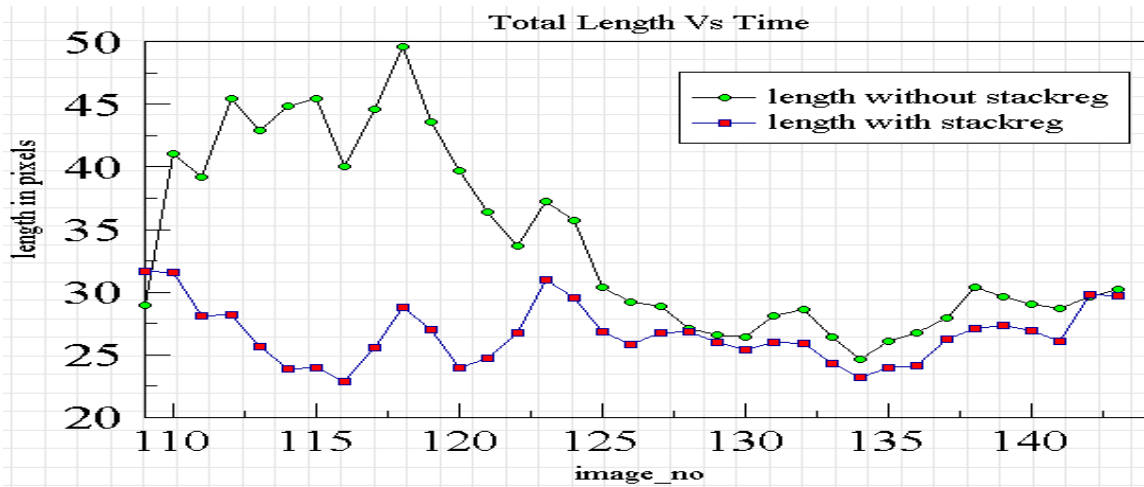
Figure 3- 8: Length and large strain with and without stack registration

The fibril which was stack registered had a length ranging from 22 to 33 pixels whereas the fibril which was analyzed without the registration process indicated a length varying from 28 to 50 pixels. This difference in the lengths occurs because of the rigid body motion of the entire imaging field as a result of "camera shake" rather than representing true fibril motion. Without stack registration, the fibril lengths and displacements are likely to be overestimated. It is therefore important to correct for rigid body motion before performing the 2D DIC analysis on the movie stacks.

CHAPTER4.

RESULTS AND ANALYSIS

This chapter presents the simulations that have been performed on two different sets of movie stacks. There are two sets of movies which were collected in experiments named FN_24 and FN_12. The results of the two movie sets are presented in two different modules in this chapter.

The first module presents the large strains, displacements and total lengths of different fibrils for two different movies from experiment FN_24. The duration of the time lapse imaging in experiment FN 24 was 48 hours. The segment from 0-12 hours was not analyzed in this study because there was significant amount of new fibril formation. Since the 2D DIC software works by tracking image features, it does not perform well on image stacks where there is too much change in image features between frames. The 2D DIC analysis was run on the movie segment from 12-48 hours to determine the dynamic nature of the fibril motion over time and measure changes in their dynamic behavior that may be related to maturation of the ECM. Data generated from the 2D DIC analysis for the 12-48 hour period was then divided into three 12 hour segments to compare results at different stages in the fibril assembly time course.

The second module discusses the strains and displacements on the second experiment called FN_12. The duration of the time lapse imaging in experiment FN 12 was also 48 hours. Five different movies from experiment FN 12 were analyzed over the 24-48 hour period of the movie. The 0-24 hour segment of the movie was not analyzed in this study due to significant amount of new fibril formation during 0-12

hours and a lot of breaking and joining of fibrils in the 12-24 hour segment. Therefore, due to the rapid change in image features between movie frames, these movie segments are not well suited for the 2D DIC analysis.

4.1   FN_24 Analysis:

Two different imaging fields were analyzed for FN_24 which are termed as position 14 and position 15. The time lapse image stack was collected from a 48 hour experiment where images were captured every 15 minutes which gives us a total of 192 frames for each movie or position. The movie was stack registered to correct for rigid body motion and the stack was converted to an RGB image with only the red color component. The brightness and contrast were also adjusted to perform better correlation. The 2D DIC analysis was performed on the 12-48 hour period of the movie, as explained above.

The first analysis was performed on position 14 from 12-48 hours which includes the image frames from 48 to 192. Figure 4.1 shows a movie animation in the electronic PDF version of the correlation process on the fibrils which starts from the base image that is frame number 48 which was used to select the fibrils and position the raster points. A total of 10 fibrils were selected for this analysis and the raster points were positioned based on the protocol developed in chapter 3 (i.e. 1 raster point for every 5 pixels of fibril length).

After we select the fibrils and mark the raster points for each fibril the normalized cross correlation analysis was performed with respect to the previous image i.e. the iteration starts with the base image as image 48 and current image as image 49 and this iteration stops when the base image is image 191 and current image is image

192. Then the total length and the large strains on each individual fibril were calculated.

These data are presented in figure 4.2.
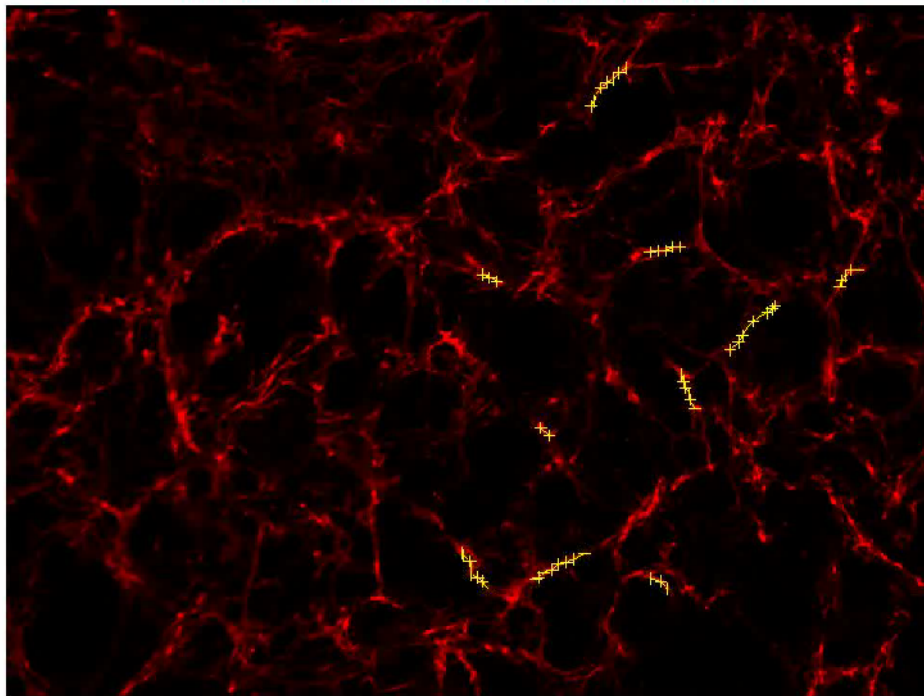
Figure 4- 1: Correlation of fibrils from 12-48hr for 10 fibrils in FN 24 at position 14

Total Length (pixels)

Large strain (με)

Image number

Image number

42

Total Length (pixels)

Large strain (με)

Image number

Image number
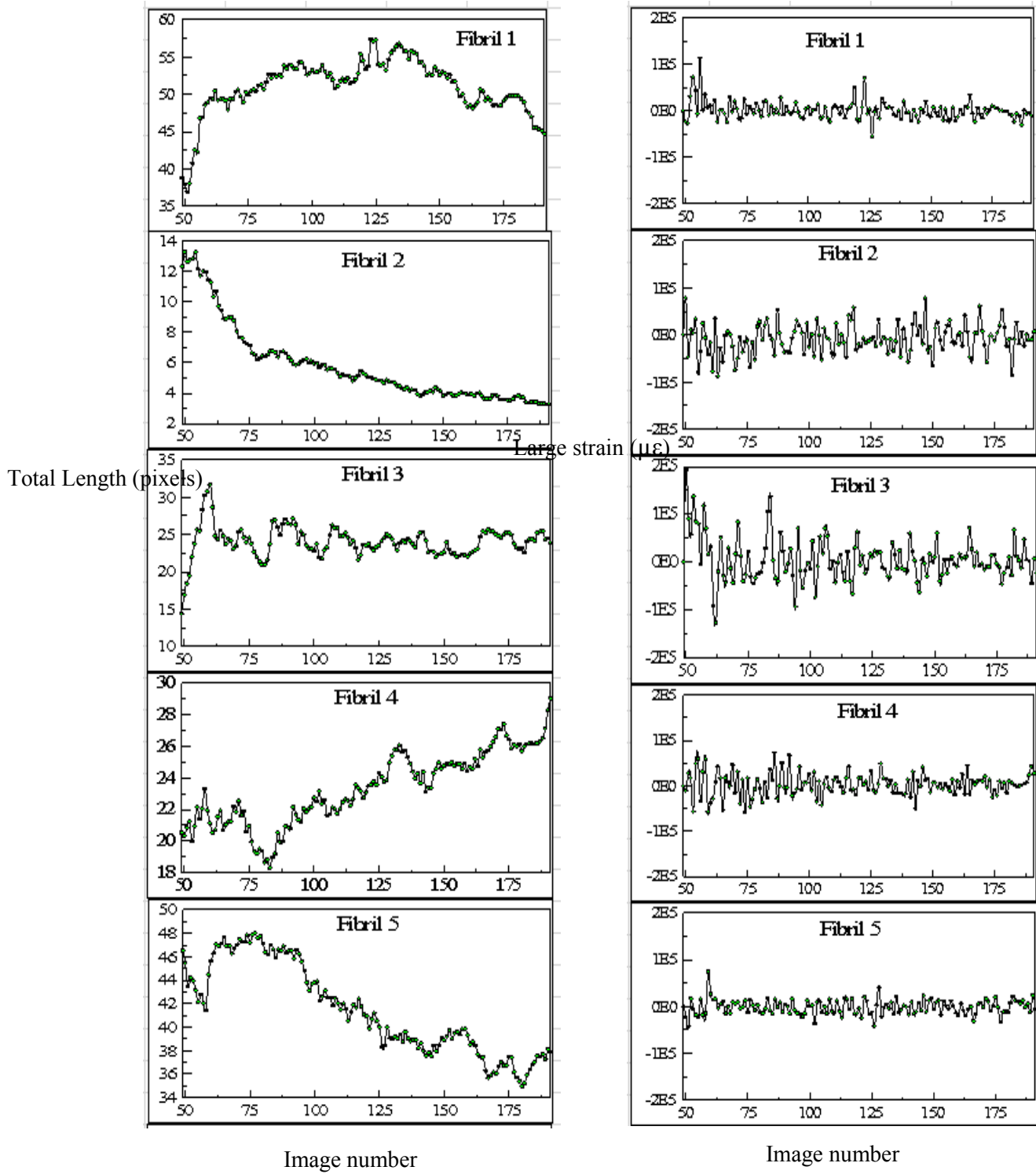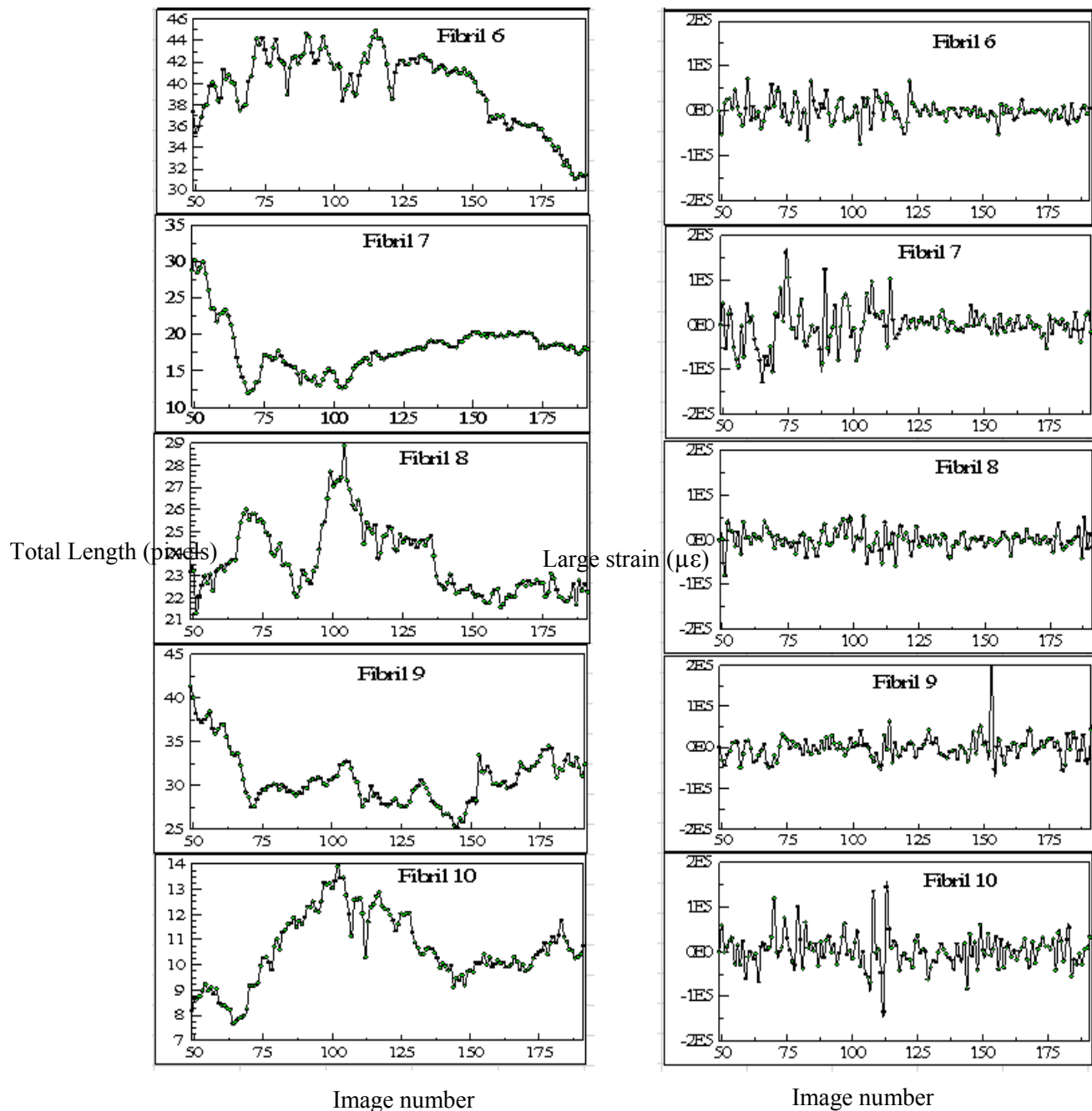
Figure 4- 2: Individual lengths and large strains for 10 fibrils in FN 24 at position 14

43

From figure 4-2 we can observe that the total lengths and the large strain for all the ten fibrils selected for the correlation analysis over 12-48 hours of the experiment. Note that individual fibrils show unique strain profiles, but that all fibrils experience both tensile and compression forces over the time course. Fibrils 3, 4, 6, 7 and 10 experience larger order tensile and compression forces during the 12-24 hour segment of the experiment (image frames 49-96) compared to the later 24-36 hour and 36-48 hour segments (image frames 97-144 and 145-192, respectively). There is also a decrease in the large strain values towards the end of the imaging period for fibrils 1, 2, 3, 4, 6, 7 and 10. This may reflect maturation of the matrix and/or reduced cell motility in the 24-48 hour period resulting in less fibril deformation.

Tables 4-1 and 4-2 provide the statistics of all ten fibrils that were used for the correlation. The tables divide the analyzed portion of the movie into three 12 hour segments (12-24hr, 24-36hr and 36-48hr) and describe the average lengths and the average tensile/compression strains for each of these stages during the time course of fibronectin fibril assembly. Table 4-1 gives the average and standard deviation values of the tensile strain for all 10 fibrils, and Table 4-2 contains the average and standard deviation values of the compression strains for the same ten fibrils. The first column in both the Table 4-1 and Table 4-2 has the fibril number with their respective number of raster points used for correlation that has been derived from the calculated physical length of the particular fibril in the first frame and following the protocol developed in chapter 3.

Table 4- 1: Tensile large strain statistics for 10 fibrils in FN 24 at position 14 in each 12hr

Fibril Number (Raster Point Density)/Physical length first frame	Length (Pixels)	Tensile Large Strain (με)		
		12-24hr	24-36hr	36-48hr
	Avg	Avg	Avg	Avg
1 (8RP)/40	51	21286	12601	7870
2 (3RP)/14	6	23308	25215	20958
3 (3RP)/14	24	62511	29432	18892
4 (5RP)/23	23	28444	18187	13671
5 (9RP)/45	42	13155	12790	11244
6 (9RP)/42	40	24211	18267	6762
7 (6RP)/31	18	48512	27450	15446
8 (5RP)/22	24	16450	18747	10263
9 (9RP)/48	31	13198	16712	25939
10 (2RP)/12	11	27673	32517	21915

Table 4- 2: Compression large strain statistics for 10 fibrils in FN 24 at position 14 in each 12hr

Fibril Number (Raster Point Density)/ Physical length first frame	Length (Pixels)	Compression Large Strain (με)		
		12-24hr	24-36hr	36-48hr
	Avg	Avg	Avg	Avg
1 (8RP)/40	51	-10406	-14131	-11630
2 (3RP)/14	6	-34258	-23852	-24265
3 (3RP)/14	24	-36609	-24721	-19657
4 (5RP)/23	23	-28343	-16546	-10720
5 (9RP)/45	42	-12864	-14583	-11446
6 (9RP)/42	40	-23299	-17562	-13359
7 (6RP)/31	18	-47833	-18863	-14269
8 (5RP)/22	24	-17144	-20234	-13373
9 (9RP)/48	31	-20912	-16847	-22725
10 (2RP)/12	11	-22305	-28883	-27250

The statistics of these fibrils are graphically depicted in figure 4.3 which is a plot of the average tensile and compression strain of each individual fibril corresponding to their average length.
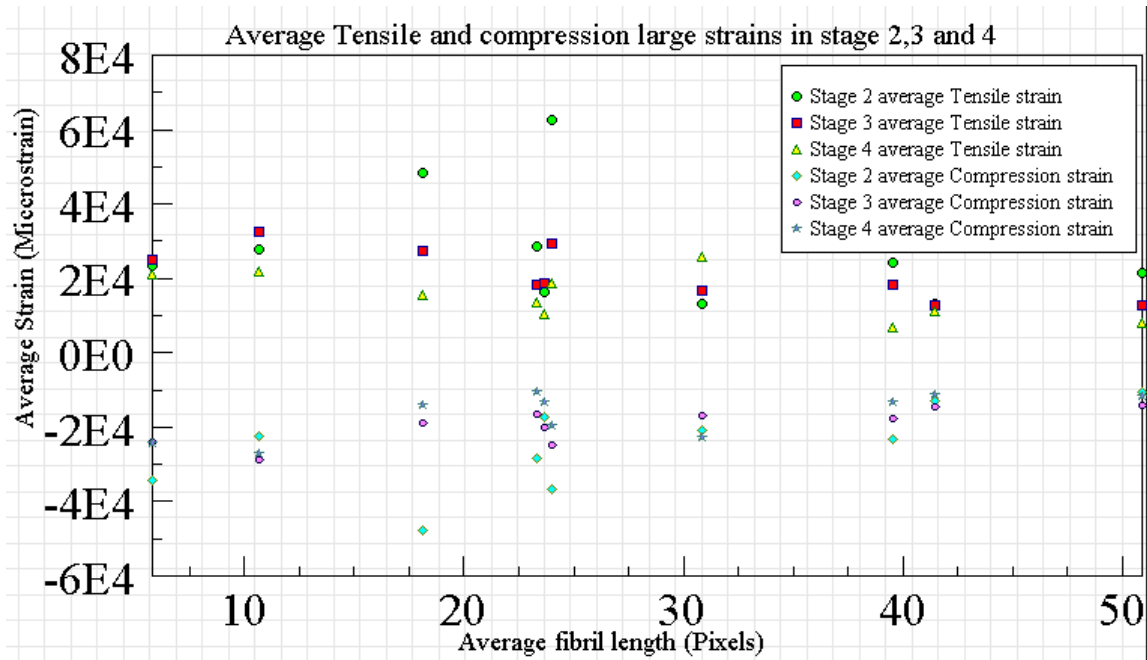
Figure 4- 3: Average tensile and compression strains for 10 fibrils in all 3 stages in FN 24 at position 14

We can observe from the figure 4-3 that for most of the fibrils the average tensile and compression strains are at their peak value during the12-24hr period of the experiment (stage 2) which is represented by a circle for tensile strains and rhombus for compression strains respectively. This suggests either that the fibrils are subjected to larger forces in this earlier period due to the underlying cell motion or that there are changes in the mechanical properties of the fibronectin fibrils with maturation that result in deformation. Very few fibrils show the same range of strains at all stages of the experiment which means that these fibrils are being subjected to uniform forces throughout the experiment.

In FN 24- position 14 at stage 2, 3 and 4 the average tensile strains is 27,000 µε,

21,000 µε and 15,000 µε; whereas the compression strain values are -25,000 µε, -19,000

µε and -16,000 µε. To get a clearer picture of the strains at different stages we averaged

the means of the tensile and compression strains of the ten fibrils for each 12 hour
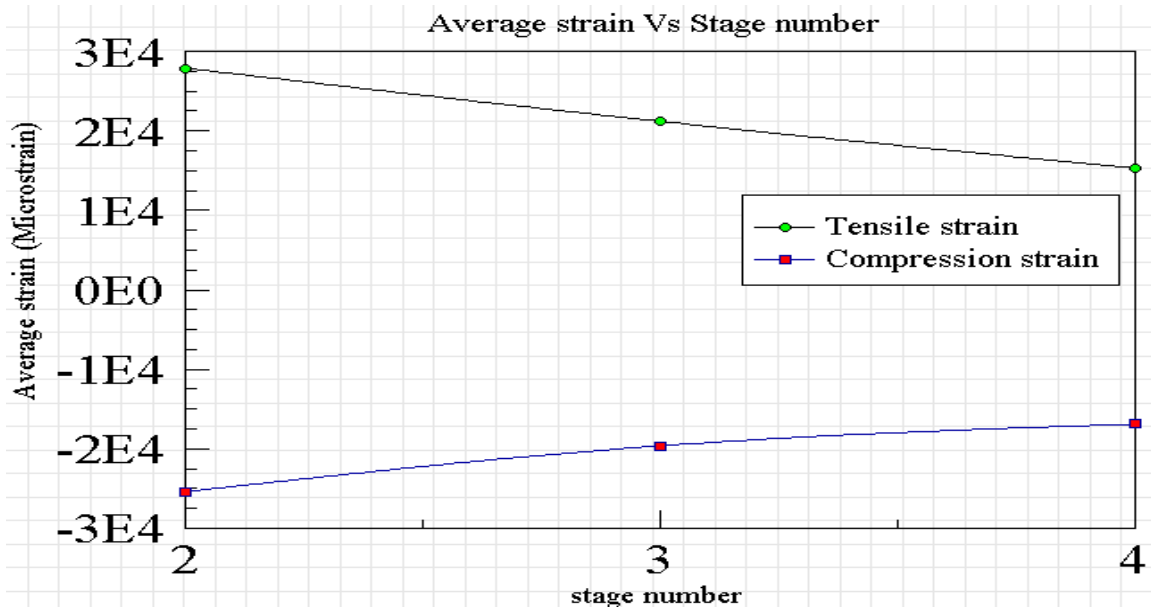
Figure 4- 4: Stage number versus the average strain for FN 24 at position 14

segment of the analysis separately and generated a graph which shows the average strains

versus the stage number as shown in figure 4.4.

We can clearly observe that the tensile/compression strains of the fibrils reduce

as time increases which suggests matrix maturation and/or reduced cell motility over

time. The tensile and compression strains are reduced by a magnitude of 6,000 µε from

12-24hr (stage 2) to 24-36hr (stage 3). In contrast, from 24-36hr (stage 2) to 36-48hr

(stag 3) the compression strain reduces by only 3,000 µε while tensile strain reduces by

the same magnitude of 6,000 µε. Overall, for position 14 of the FN_24 experiment the

tensile strains are reduced by 12,000 με by the end of experiment whereas the compression strains are reduced by 9,000 με.

Table4-3 shows the statistics of the same above 10 fibrils in experiment FN 24, position 14 but here the average tensile and compression large strains were calculated for the complete 12-48hr movie period rather than dividing the data into 12hr movie segments. The peak tensile and compression strains are also shown.

Table 4- 3: Statistics of 10 fibrils in FN 24 at position 14 for 12-48h movie period

Statistics/Physical length		Length(Pixels)			Tensile Large strain (με)		Compression Large strain(με)	
		Average	Min	Max	Average	Peak	Average	Peak
fibril number (Raster point density)	1(8RP)/40	51	37	57	14609	113683	-10406	-26991
	2(3 RP)/14	6	3	13	22923	78594	-34258	-88125
	3(3 RP)/14	24	14	32	37258	193324	-36609	-125931
	4(5RP)/23	23	18	29	19607	73089	-28343	-58392
	5(9RP)/45	42	35	48	12339	75255	-12865	-43183
	6(9RP)/42	40	31	45	17425	71383	-23299	-66440
	7(6 RP)/31	18	12	30	28655	162540	-47834	-128312
	8(5 RP)/22	24	21	29	14997	53497	-17144	-79678
	9(9RP)/48	31	25	41	19387	198970	-20912	-48996
	10(2 RP)/12	11	8	14	26857	146279	-22305	-66876

Tables 4-1, 4-2 shows the tensile/compression strains either for each individual stages of the experiment i.e. stage2,3 or 4 and Table 4-3 presents the strain data for the all the stages combined as a total(stage 2 to 4), but the shared feature in all these three tables is that the strains are measured with respect to previous image i.e. in this particular

48

experiment there are 146 images correlated and strains on fibril between each consecutive image is computed and the average and peak of all these successive frames is calculated and tabulated in Table 4-3. Now this gives us information regarding the peak and average strains experienced by the fibrils with respect to previous image in the analysis. We can also perform correlation with respect to first image or base image and calculate the strains with respect to first image. These two different analyses represent two different kinds of data, but from Aditya's thesis it was concluded that it is better to use correlation with respect to previous image rather than first image for this particular application of strain calculation.

The same analysis was repeated for position 15 of the FN_24 experiment, where 15 fibrils were selected for 2D DIC with respect to the previous image. The data were divided into three 12 hour segments as before. The statistics for these fibrils are presented in table 4-4 and 4-5.

Table 4- 4: Tensile large strain statistics for 15 fibrils in FN 24 at position 15

Fibril Number (Raster Point Density)/ Physical length first frame	Length (Pixels)	Tensile Large Strain (με)		
		12-24hr	24-36hr	36-48hr
	Avg	Avg	Avg	Avg
1(2 RP)/12	7	21958	43188	51903
2(2 RP)/10	7	24450	14024	13344
3(4 RP)/22	16	29102	24779	25028
4(4 RP)/21	14	14782	23237	18226
5(4 RP)/21	20	12417	9922	13224
6(7 RP)/34	35	18168	19807	12902
7(5 RP)/26	25	30241	20703	22065
8(10 RP)/48	52	17450	12967	8899
9(7 RP)/36	31	16100	15464	11634
10(10 RP)/50	58	14054	10782	7616
11(2 RP)/12	11	31891	38525	26759
12(3 RP)/14	13	40471	20968	23184
13(3 RP)/14	10	29112	18777	20240
14(3 RP)/16	11	23526	22054	23991
15(7 RP)/36	29	22285	13947	24619

Tables 4-4 and 4-5 provide the statistics for all the fifteen fibrils that were used for the correlation. They describe the average lengths and the average tensile (Table 4-4) compression (Table 4-5) strains for each individual stage (12-24hr, 24-36hr, 36-48hr) of the movie.

Table 4- 5: Compression large strain statistics for 15 fibrils in FN 24 at position 15

Fibril Number (Raster Point Density)/ Physical length first frame	Length (Pixels)	Compression Large Strain (με)		
		12-24hr	24-36hr	36-48hr
	Avg	Avg	Avg	Avg
1(2 RP)/12	7	-29250	-39694	-32809
2(2 RP)/10	7	-23963	-15139	-16083
3(4 RP)/22	16	-45051	-23722	-21378
4(4 RP)/21	14	-29300	-20866	-20780
5(4 RP)/21	20	-15036	-13963	-17428
6(7 RP)/34	35	-20719	-22424	-14999
7(5 RP)/26	25	-38623	-18494	-18159
8(10 RP)/48	52	-9846	-13957	-7701
9(7 RP)/36	31	-18782	-15523	-12016
10(10 RP)/50	58	-15488	-11071	-10788
11(2 RP)/12	11	-30079	-26104	-22113
12(3 RP)/14	13	-38603	-15271	-16901
13(3 RP)/14	10	-34988	-20926	-18213
14(3 RP)/16	11	-20846	-14280	-27759
15(7 RP)/36	29	-23216	-19023	-21673

The statistics of these fibrils are graphically depicted in figure 4-5 which is a plot of the average tensile and compression strain of each individual fibril corresponding to their average length.
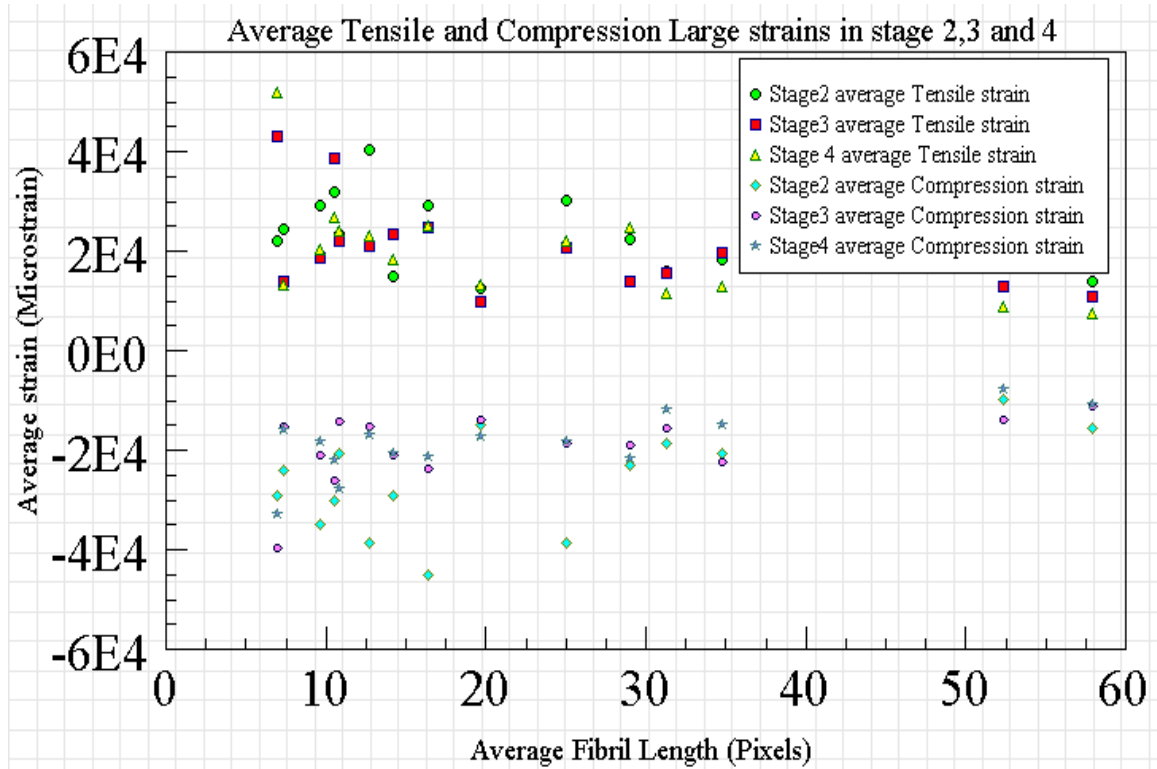
Figure 4- 5: Average tensile and compression large strain in all 3 stages for FN 24 at position 15

We can again observe that for most of the fibrils the average tensile and compression strains are at their peak value during the12-24hr of the experiment (stage 2), and that the strains are reduced for the same fibrils during the 24-36hr period (stage 3) and 36-48hr period (stage 4) of the experiment. Very few fibrils show the same range of fibrils at all stages of the experiment which means that these fibrils are being subjected to uniform forces throughout the experiment.

In FN 24 at position 15 at stage 2, 3 and 4 the average tensile strains values are 23,000 με, 20,000 με and 19,000 με respectively; whereas the compression strain values are -26,000 με, -19,000 με and -18,500 με.

To get a clear picture of the strains at the different stages we averaged the means of the tensile and compression strains of the fifteen fibrils for each 12 hour segment of the analysis separately and generated a graph which shows the average strains versus the stage number as shown in figure 4-6.
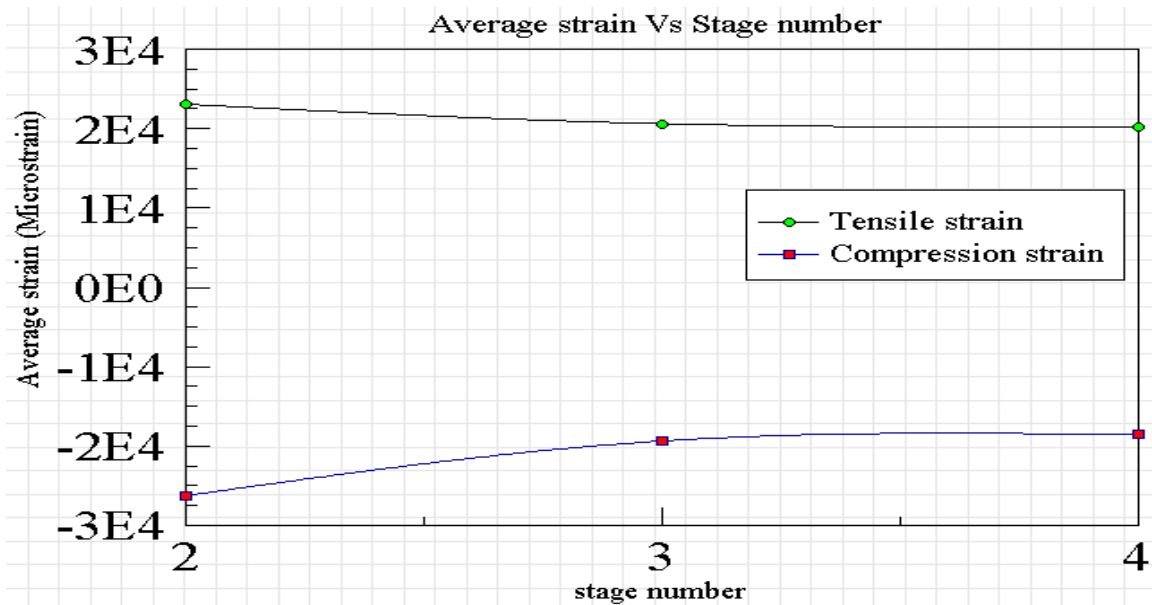
Figure 4- 6: Average strain versus stage number for FN 24 at position 15

We can again observe that the tensile/compression strains of the fibrils reduce as time increases. For position 15, the tensile and compression strains are reduced by a magnitude of 3,000 $\mu\varepsilon$ and 7,000 $\mu\varepsilon$ respectively from 12-24hr (stage 2) to 24-36hr (stage 3). From 24-36hr (stage 3) to 36-48hr (stage 4) the compression strain reduces by only 1,000 $\mu\varepsilon$ whereas the tensile strain reduces by 1,500 $\mu\varepsilon$ at all. By this we can observe that for different positions of the same experiment the strains change differently as the matrix matures due to biological variations.

4.2 FN_12:

This section introduces the analysis that has been performed on position 9,10,11,12 and 16 from experiment FN_12. These time lapse image stacks were collected from a 48 hour experiment where the images were captured for every 20 minutes which gives us a total of 144 frames in each position. The movie was stack registered and the stack was converted to RGB image with only the red color component. The brightness and contrast were also adjusted for better correlation. The 2D DIC analysis was performed on the 24-48hr period of the movies from experiment FN_12 in contrast to FN_24 where we analyzed from 12-48 hours as FN_12 showed significant new fibril formation in the first 12hr period, which continued through 12-24hr (stage 2), resulting in dynamic change in the image features, which is difficult for the DIC algorithm to track.

The first analysis was performed on position 9 from 24-48 hour which includes image frames from 72 to 144. Figure 4-7 shows an animated movie of the correlation process on the fibrils which starts from the base image that is frame number 48, which was used to select the fibrils and position the raster points. A total of 10 fibrils were selected for this analysis and the raster points were positioned based on the protocol developed in chapter 3 (i.e.1 raster point for every 5 pixels of fibril length). First the physical length of the fibril was measured manually in the base image and then the raster points were positioned.
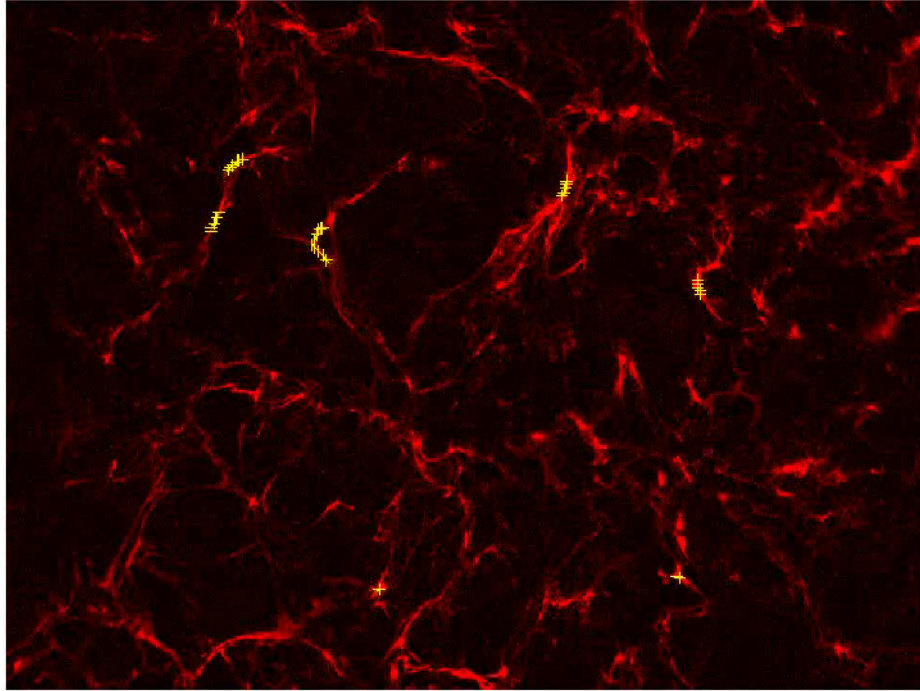
Figure 4- 7: Base image of FN 12 at position 9

After we selected the fibrils and marked the raster points for each fibril the normalized cross correlation analysis was performed with respect to the previous image i.e. the iteration starts with the base image as image 72 and current image as image 73 and this iteration stops when the base image is image 143 and current image is image 144. Then the total length and the large strains on each individual fibril were calculated.

Table 4-6 provides the statistics for all the ten fibrils that were used for the correlation. It divides the analyzed portion of the movie into two 12 hour segments,

55

stages 3 and 4, which represent 24-36hr and 36-48hr, respectively. The table describes the average lengths and the average tensile/compression strains for each of these stages in the time course of fibronectin fibril assembly.

Table 4- 6: Statistics of average tensile and compression strain in each stage in FN 12 at position 9

Fibril Number (Raster Point Density)/Physical length first frame	Length (Pixels)	Tensile Large strain (με)		Compression large strain (με)	
		Stage 3	Stage 4	Stage 3	Stage 4
Avg	Avg	Avg	Avg	Avg	Avg
1 (5RP)/26	25	41551	44059	-56814	-25437
2 (7RP)/33	42	53449	24442	-26842	-13582
3 (7RP)/35	54	61304	30310	-26290	-16393
4 (2RP)/12	7	83646	16320	-37396	-23341
5 (12RP)/60	70	20072	13565	-22528	-14255
6 (9RP)/44	55	43630	18222	-27849	-22520
7 (2RP)/10	7	16107	11131	-21195	-53029

The statistics of these fibrils are graphically depicted in figure 4-8 which is a plot of the average tensile and compression strain of each individual fibril corresponding to their average length.
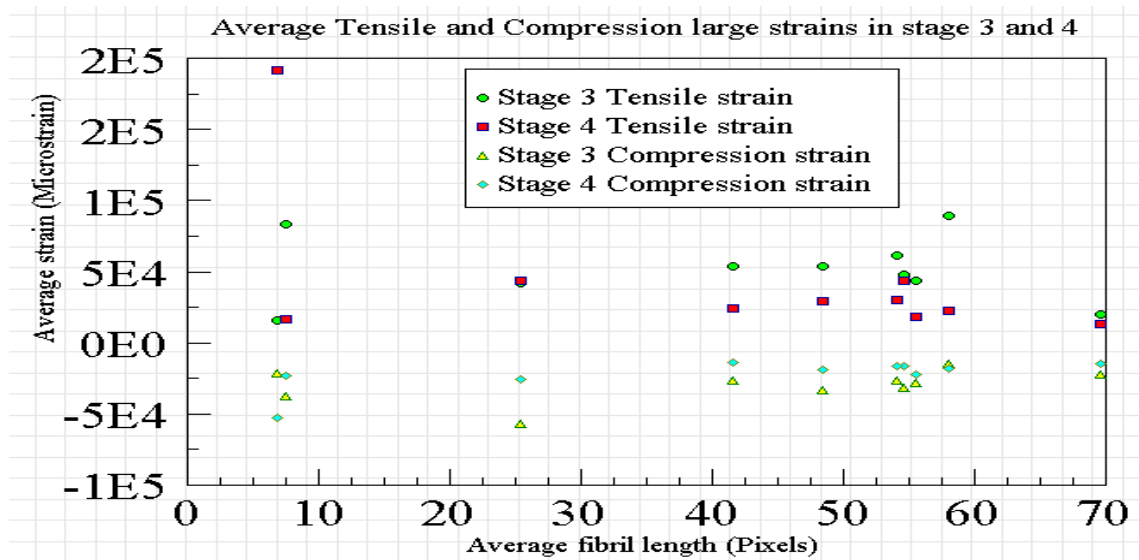
Figure 4- 8: Average strains of 10 fibrils from 24-48hr of FN 12 at position 9

The data shows that for most of the fibrils the average tensile and compression strains are higher at 24-36hr (stage 3) of the experiment which is represented by a circle for tensile strains and a rhombus for compression strains respectively, compared to the 36-48hr (stage 4). This suggests either that the fibrils are subjected to larger forces due to the cell motion, which causes more changes in length and higher strains, or that the material properties of the matrix change so that there is less deformation for the same amount of strain. Very few fibrils show the same range of fibrils at all stages of the experiment which means that these fibrils are being subjected to uniform forces throughout the experiment.

As for experiment FN_12 we averaged the means of the tensile and compression strains of the ten fibrils for each 12 hour segment of the analysis separately and generated a graph which shows the average strain versus the stage number as shown in figure 4-9.

Figure 4- 9: Stage number versus average strain for FN 12 at position 9

As observed for positions 9 in experiment FN_12, the tensile/compression strains of the fibrils reduced with time, suggesting reduced cell motility and/or matrix maturation that resulted in lower strains. The tensile and compression strains are reduced by a magnitude of 23,000 $\mu\varepsilon$ and 7,000 $\mu\varepsilon$ from 24-36hr to 36-48hr.
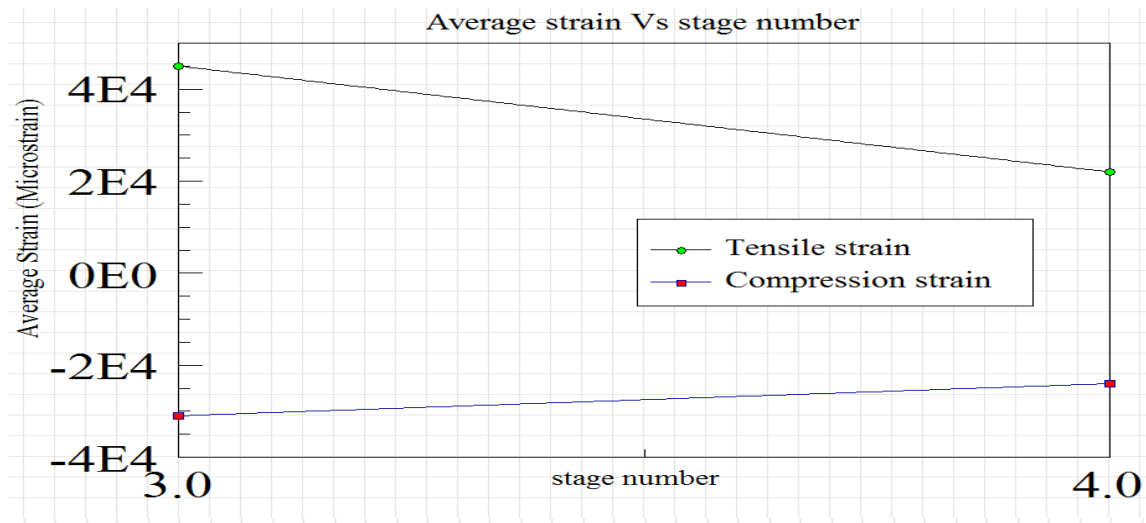
The same analysis was repeated on positions 10, 11, 12 and 16 and all the stages showed a similar decrease in tensile and compression strains as the matrix matures. Table 4-7 shows the overall average tensile and compression strain of the set of fibrils selected for correlation in the FN 12 experiment at different positions.

Table 4- 7: Average strain values for position 9, 10, 11, 12 and 16 of FN 12 Experiment

Experiment/Position (number of fibrils analyzed)	Average tensile strain		Average compression strain	
	24-36hr	36-48hr	24-36hr	36-48hr
FN 12/Position 9 (7)	45,000	22,000	-31,000	-24,000
FN 12/Position 10 (6)	34,000	22,000	-29,000	-20,000
FN 12/Position 11 (7)	70,000	29,000	-36,000	-25,000
FN 12/Position 12 (4)	84,000	38,000	-40,000	-41,000
FN 12/Position 16 (4)	57,000	34,000	-51,000	-33,000

We can observe from Table 4-7 that positions 11, 12 and 16 shows a decrease of 25,000 to 35,000 $\mu\varepsilon$ of tensile strain from 24-36hr to 36-48hr of the experiment which is very high and position 10 shows a low decrease of strains. This table is graphically depicted in the following Figure: 4-10.
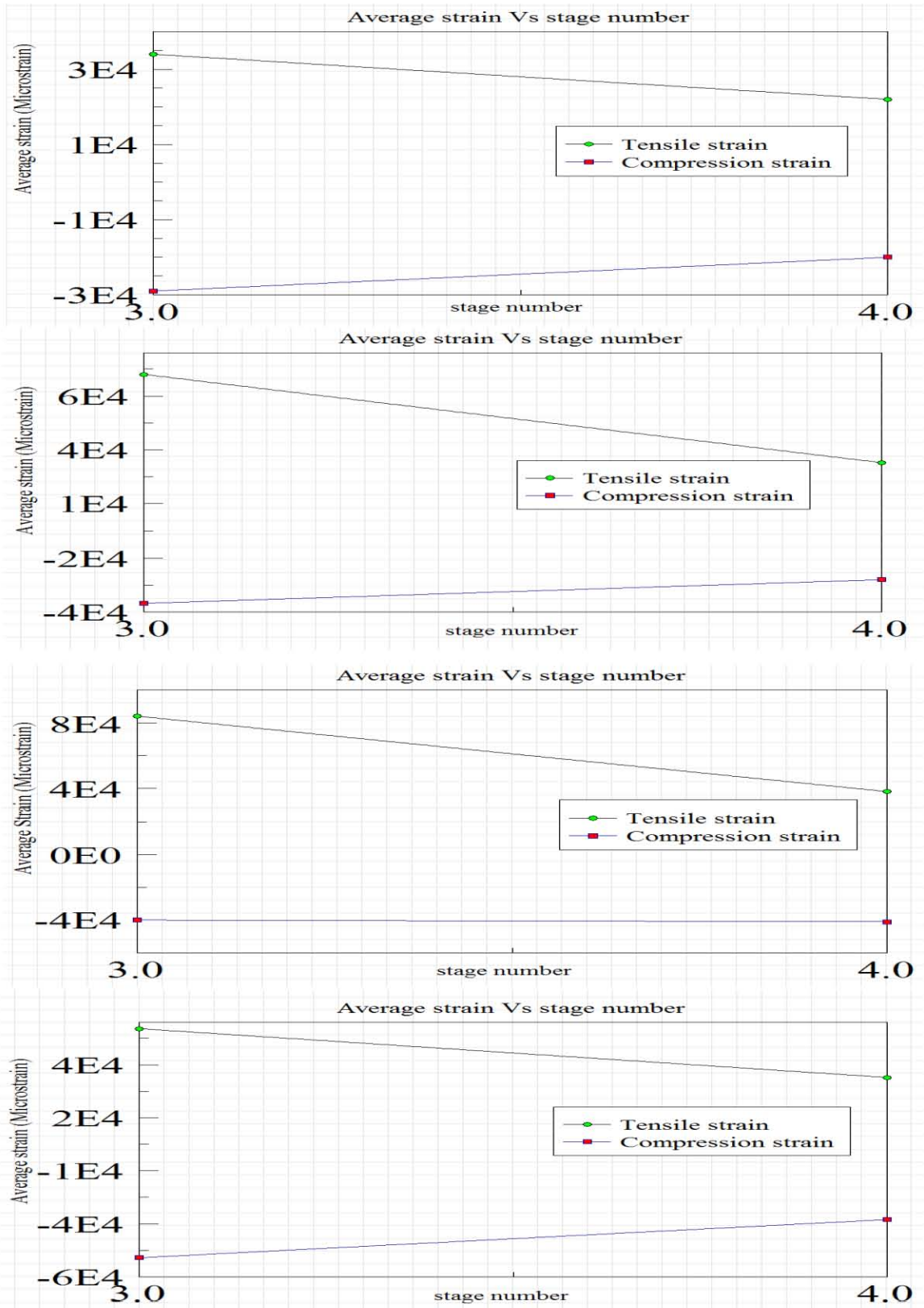
Figure 4- 10: Stage number versus average strain for FN 12 at position 9

CHAPTER5.

CONCLUSIONS AND FUTURE WORK

This chapter gives the conclusion from the analyses performed on the two different fibronectin live imaging experiments at seven different imaging positions. This research has effectively developed the Matlab code to perform a modified digital image correlation which suits this particular application. We have been successful in developing a protocol for analysis of fibronectin fibril strains from time lapse movie data based upon using an optimal number of raster points per unit of fibril length and upon applying image processing steps such as stack registration, conversion to RGB image and brightness and contrast adjustments.

The main conclusion of this research is that the fibronectin assembly process is very dynamic and that the forming fibronectin fibrils are subjected to considerable forces generated by the underlying motion of 2T3 cells.

From the statistics of the fibril strains from the different positions of the experiments we can observe that each individual fibril has its unique strain profile and unique lengths but all the fibrils experience both the tensile and compression forces. The absolute value of the average tensile/compression strains of the fibronectin fibrils range from 17,000 $\mu\varepsilon$ to 78,000 $\mu\varepsilon$ depending on the time and position of the experiment, but the peak strains of each fibril is twice the average strains which could be due to sudden decrease or increase length.

The data suggests that the strains experienced by fibronectin fibrils due to the motile 2T3 osteoblast cells are 10-20 times the strains experienced on bone surfaces that are subjected to mechanical loading.

This suggests the significance of the fibronectin fibrils in the assembly of bone ECM as we could observe the continual presence of the fibronectin fibril in the cellular interactions in the ECM assembly process, and these cellular interactions are the basis of for fundamental biological processes.

Taken together, the data from experiments FN_24 and FN_12 show that the fibronectin fibril strain values decrease with time. Since the fibronectin fibril deformation occur as a result of cell motion, this decrease in strain with time may reflect a reduction in cell motility and/or ECM maturation, such as crosslinking of matrix molecules. This ECM maturation could alter the mechanical properties of the ECM such that there is lower deformation.

The future work of this research is based on the drawbacks of coding section of this application. The work can be organized as follows:

1.   We need to develop a GUI (Graphical User Interface) based application where all the different m files of the Matlab can be simulated at one single click rather than the user running each and every m file and organizing the output. This gives the user the flexibility for effective simulation.

2.   Another important feature that can be added to the existing code is to improve the way the results are organized. If the results are stored in a much more effective way rather than storing in the .dat files it would be easier for the user to understand and analyze the results rather than spending time to organize the results.

3.   A very important future direction of the research is to develop a correlation technique using Matlab that can be used to track fibrils even during the first stages of the experiment where there is a large amount of new fibril assembly, together with extensive fibril motion and breaking/joining of fibrils. This rapid degree of change and the "birth" of new image features during the movie makes it very difficult for the 2D DIC algorithm to accurately track image features.

4.   The work would also be strengthened by adding in the ability to track the cell motions related to the fibril assembly and quantify the cell motion and relate it to the fibril motion.

5.   In vivo confirmation of the results, which have so far been generated using in vitro cell culture systems, would also be a future research goal, since it will be important to determine whether fibronectin assembly in the whole organism occurs by similar mechanisms.

6.   Trying to implement a advanced code which identifies the fibrils that do not track well by creating a threshold on window correlation size and remove these fibrils while quantifying the results.

7.   A drawback of this thesis is the optimum raster point number which is 1 RP per 5 pixels can be modified by doing more number of simulations(with more raster points) and then performing a linear regression model that will provide a much effective and accurate result.

8.   Another feature that can be added is to develop the code in such a way that we can draw the contour of the fibril in the first image and the program should

automatically calculate the optimum RP density and place the points in such a way that we don't lose the fibril length information.

BIBLIOGRAPHY

Biomedical Imaging Group. (2011, July 7). Retrieved from Biomedical Imaging Group: http://bigwww.epfl.ch/thevenaz/stackreg/

Live Cell Imaging. (2014, 03 22). Retrieved 05 21, 2014, from Wikipedia: http://en.wikipedia.org/wiki/Live_cell_imaging

Brillaud, J., & Lagattu, F. (2002). Limits and possibilities of laser speckle and white-light image-correlation methods: theory and experiments. *Applied Optics, 41*(31), 6603-6613.

Czirok, A., Zach, J., Kozel, B. A., Mecham, R. P., Davis, E. C., & Rongish, B. J. (2006). Elastic fiber macro-assembly is a hierarchical, cell motion process. *Journal of Cellular Physiology, 207*(1), 97-106.

Dallas, S. L., Chen, Q., & Sivakumar, P. (2006). Dynamics of assembly and reorganization of extracellular matrix proteins. *Current topics in Developmental Biology, 75*, 1-24.

Dallas, S. L., Veno, P. A., Rosser, J. L., Barragan-Adjemian, C., Rowe, D. W., Kalajzic, I., & Bonewald, L. F. (2009). Time lapse imaging techniques for comparison of mineralization dynamics in primary murine osteoblasts and the late osteoblast/early osteocyte-like cell line MLO-A5. *Cells Tissues Organs, 189*, (1-4),6-11.

Eberl, C., Thompson, R., & Gianola, D. (2006, September 27). *Matlab Central*. Retrieved from Mathworks: http://www.mathworks.com/matlabcentral/fileexchange/12413-digital-image-correlation-and-tracking

Filla, M. B., Czirok, A., Zamir, E. A., Little, C. D., Cheuvront, T. J., & Rongish, B. J. (2004). Dynamic imaging of cell, extracellular matrix, and tissue movements during avian vertebral axis patterning. *Birth Defects Research Part C: Embryo Today: Reviews, 72*(3), 267-276.

Friedl, P. (2004). Dynamic imaging of cellular interactions with extracellular matrix. *Histochemistry and Cell Biology, 122*(3), 183-190.

Hung, P. C., & Voloshin, A. S. (2003). In-plane strain measurement by digital image correlation. *Journal of the Brazilian Society of Mechanical Sciences and Engineering, 25*(3), 215-221.

Kim, K. C., Yoon, S. Y., Kim, S. M., & H. H. Chun, I. L. (2006). An orthogonal-plane PIV technique for the investigations of three-dimensional vortical structures in a turbulent boundary layer flow. *Experiments in Fluids, 40*(6), 876-883.

Kozel, B. A., Rongish, B. J., Czirok, A., Zach, J., Little, C. D., Davis, E. C., . . . Mecham, R. P. (2006). Elastic fiber formation: A dynamic view of extracellular matrix assembly using timer reporters. *Journal of Cellular Physiology, 207*(1), 87-96.

Lewis, J. P. (1995, May). Fast Normalized cross-Correlation. *Vision Interface, 10*(1), 120-123.

Lu, H., & Cary, P. D. (2000). Deformation measurements by digital image correlation: Implementation of a second-order displacement gradient. *Experimental Mechanics, 40*(4), 393-400.

McCormick, N., & Lord, J. (2010). Digital image correlation. *Materials today, 13*(12), 52-54.

65

McNeill, S. R., Peters, W. H., & Sutton, M. A. (1987). Estimation of stress intensity factor by digital image correlation. *Engineering Fracture Mechanics, 28*(1), 101-112.

Pan, B., Qian, K., Xie, H., & Asundi, A. (2009). Two- dimensional digital image correlation for in-plane displacement and strain measurement: a review. *Measurement Science and Technology, 20*(6), 062001.

Pan, B., Xie, H., Wang, Z., & Qian, K. (2008). Study on subset size selection in digital image correlation for speckle patterns. *Optics Express, 16*(10), 7037-7048.

Pankov, R., & Yamada, K. M. (2002). Fibronectin at a glance. *Journal of Cell Science, 115*(20), 3861-3863.

Roshan, A. (2011). Deformation mapping of fibronectin fibrils using digital image correlation.

Schreier, H. W., & Sutton, M. A. (2002). Systematic errors in digital image correlation due to undermatched subset shape functions. *Experimental Mechanics, 42*(3), 303-310.

Sivakumar, P., Czirok, A., Rongish, B. J., Divakara, V. P., Wang, Y. P., & Dallas, S. L. (2006). New insights into extracellular matrix assembly and reorganization from dynamic imaging of extracellular matrix proteins in living osteoblasts. *Journal of Cell Science, 119*(7), 1350-1360.

Sottile, J., & Hocking, D. C. (2002). Fibronectin Polymerization Regulates the Composition and Stability of Extracellular Matrix Fibrils and Cell-Matrix Adhesions. *Molecular Biology of the Cell, 13*(10), 3546-3559.

Sutton, M. A., Mingqi, C., Peters, W. H., Chao, Y. J., & McNeill, S. R. (1986). Application of an optimized digital correlation method to planar deformation analysis. *Image and Vision Computing, 4*(3), 143-150.

Thévenaz, P. (2011, July 7). *Stack Registration*. Retrieved from Biomedical Imaging Group: http://bigwww.epfl.ch/thevenaz/stackreg/

Velling, T., Risteli, J., Wennerberg, K., Mosher, D. F., & Johansson, S. (2002). Polymerization of type I and III collagens is dependent on fibronectin and enhanced by integrins α11β1and α2β1. *Journal of Biological Chemistry, 277*(40), 37377-37381.

Zamir, E. A., Czirok, A., Rongish, B. J., & Little, C. D. (2005). A Digital image-based method for computational tissue fate mapping during early avian morphogenesis. *Annals of Biomedical Engineering, 33*(6), 854-865.

VITA

Bhargav Javvaji was born in January 25th 1990 in Vijayawada, Andhra Pradesh, India. He finished all his schooling in Vijayawada. Given his keen interest to become an Engineer from his childhood, he earned a bachelor's degree in technology with Electronics and Communications Engineering as his major. He graduated from Jawaharlal Nehru Technological University in the year 2011.

Bhargav moved to United States to pursue his master's degree in Electrical Engineering at University of Missouri-Kansas City in the fall term of 2011. He began his research on Image processing application on Biomedical Images with Dr. Ganesh Thiagarajan in 2012 as part of his master's degree. Upon earning his master's degree he plans to continue his research in the future.